The paper describes a technique for estimating the LWP in stratiform precipitation. The methodology is applied to 20 case studies collected during MC3E. The paper is generally clear and well written and targets a very important issue, the partitioning between cloud and rain liquid contents in precipitating clouds (though it finds only a partial solution to it).

We appreciate the reviewer for his/her time and effort for reviewing this paper. Especially, the second comment really helps the first author to gain some experiences in radiative transfer calculation and get a deeper understanding on the cloud water path retrievals at (unpolarized/polarized) microwave radiometer channels. We thank him/her for the constructive comments and suggestions. The responses are in bold and black.
We also attached the revised manuscript at the end of the response to review.

Some comments 1) It must be clear from the beginning that the methodology is only capable of computing the LWP below the bright band and that the methodology is not applicable in presence of liquid above the melting layer.

Agree. The title has been changed to "Estimation of Liquid Water Path *below the Melting Layer* in Stratiform Precipitation Systems using Radar Measurements during MC3E"
Also, clarifications are added in abstract and other places.
For example, the first sentence of in the abstract changed as "In this study, the liquid water path (LWP) below the melting layer in stratiform precipitation systems is retrieved, which is a combination of rain liquid water path (RLWP) and cloud liquid water path (CLWP). "

2) The explanation on the overestimates of LWPs by radiometers is pretty convoluted (at the moment it is a full page, page 17) and needs to be simplified.

To better understand this bit in first place you could compute the extinction (and scattering) coefficients like in Fig.10 of your second reference. Clearly raindrops are much more efficient in extinguishing radiation than cloud droplets (but this depends on the size of the raindrops! so I do not agree with the 2/3 statement at line 382). Yes I agree the single scattering albedo also is much larger.

Second you could use RT computations (e.g. Eddington or a successive order approximations where you can simplify all equations because for your purpose you can neglect polarization effects and you can assume spherical particles only) to compute the TBs for the two channels used by the radiometers to show the enhancement when r-LWP instead of c-LWP is present. Fig4 of your second reference shows an example of that for 30 degrees elevation angle (here you need to repeat the computation at nadir and for the frequencies of the radiometer). But from that figure it is clear the enhancement in case of rain: compare the TBs e.g. for c-LWP=1 kg/m^2 vs r-LWP=1 kg/m^2.

Following the suggestions, we first generated Figure B as the Figure 10a in Battaglia et al. (2009). We calculated the extinction cross section per volume as a function of the drop equivolume diameter for the two frequencies/channels in MWR (23.8 GHz and 31.4 GHZ) with a T-matrix method. It is notice that the extinction cross section increases with increased diameter when the diameters are smaller than 3 mm. This indicates the extinction (cross

section) for rain drops (diameter > ~ 50 um) is much larger than that for cloud droplets (diameter < ~50 um).

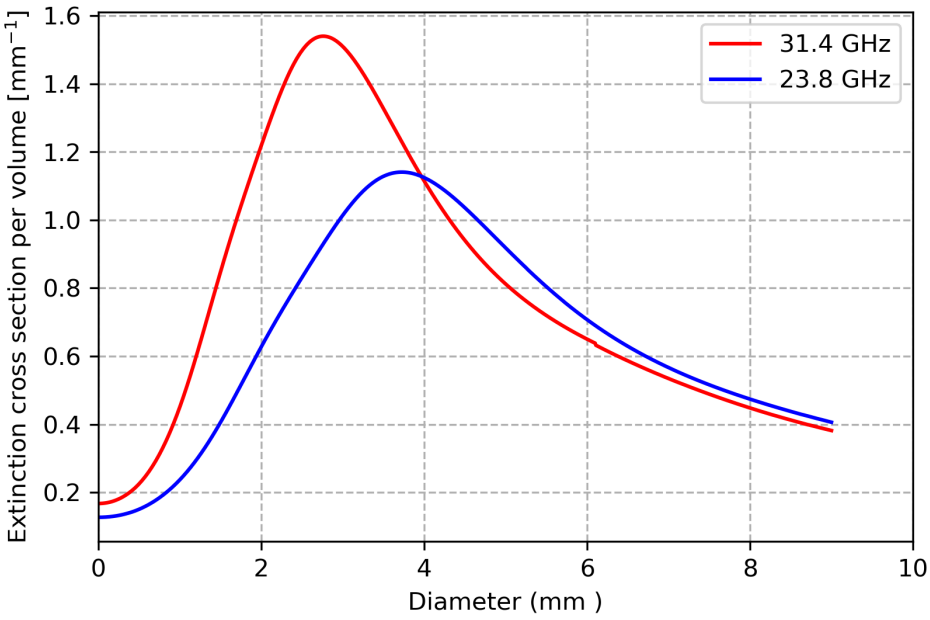

Figure B. The extinction cross section per volume as a function of the drop equivolume diameter for the two frequencies in MWR (23.8 GHz and 31.4 GHZ).

Secondly, we also generated Figure C as the Figure 10 b in Battaglia et al. (2009). We calculated the extinction coefficient as a function of RLWC for populations with three different drop size distributions (DSDs). The DSDs are modeled according to the exponential Marshall and Palmer (MP) distribution $N(D) = N_0 e^{-\Lambda D}$. N_0=8000 m^{-3} mm^{-1}. N_0 is changed to 4000 and 32000 m^{-3} mm^{-1} to represent thunderstorm and drizzle DSDs. More details of the DSDs please see Battaglia et al. (2009).

Figure C clearly shows the extinctions of cloud and rain also are DSD-dependent. For example, at 31.4 GHz, even though the RLWC is the same, the extinctions are much larger from the precipitation with the thunderstorms and MP DSDs than the extinctions from light precipitation with the drizzle DSD.

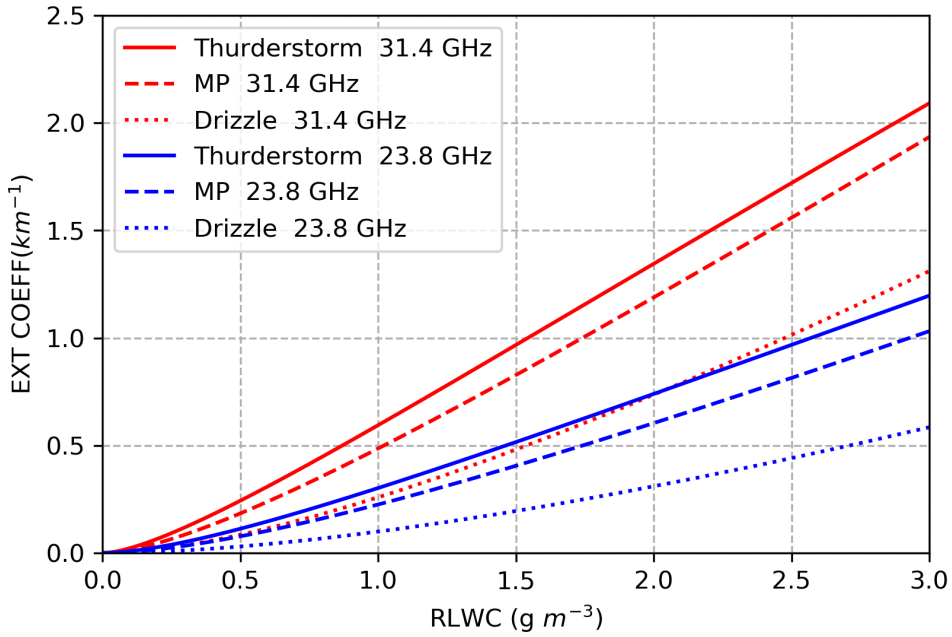

Figure C. The extinction coefficient as a function of RLWC for precipitations with three different drop size distributions (DSDs) in which they represent heavy precipitation (thunderstorm), moderate precipitation (M&P) and drizzle precipitation (drizzle).

Furthermore, we follow the suggestion to calculate the brightness temperatures at 23.8 and 31.4 GHz channels using the MicroWave Radiative Transfer (MWRT) model. Five different sensitivity tests are generated with five combinations of CLWP and RLWP values (Table A). Table A lists the results and clearly demonstrates that the brightness temperatures in channels increase with increased cloud water amount (larger CLWP) and the rain water amount (larger RLWP). Comparing the results from test #2 and #3, it is clearly seen that the brightness temperatures contributed by rain are 31 and 51 K more than that contributed by cloud at the frequencies of 23.8 and 31.4 GHz, even though their LWPs are the same (1 kg m^{-2}) in these two tests.

Table A. The brightness temperatures (TB) at 23.8 and 31.4 GHz for different assumptions of CLWP and RLWP

Sensitivity Test	CLWP (kg m^{-2})	RLWP (kg m^{-2})	TB at 23.8 GHz	TB at 31.4 GHz
#1	2	0	197.20	196.28
#2	1	0	186.34	177.49
#3	0	1	217.28	228.20
#4	0	2	254.51	272.09
#5	1	1	225.37	239.88

The figures and table listed above have been added in the Appendix B in the revision. As suggested, the explanation of overestimation of LWP from microwave radiometer is simplified in the revision. "The increase of MWR-retrieved LWP during raining periods is possibly due to the "wet radome" effect, where the deposition of raindrops on the instrument's radome can cause a large increase in the measured brightness temperatures (Cadeddu et al., 2017). In addition to the issue from standing water on the radome, the extinctions due to raindrops also affect MWR retrievals. The extinction for rain is much larger than that for cloud (Sheppard, 1996), and thus, the small amount of rain water could enhance the measured brightness temperature significantly. More details of extinctions and brightness temperature calculations at MWR channels are shown in Appendix C. "

"Appendix C: Calculations of Extinction and Brightness Temperature at Microwave Radiometer Channels

To better explain the "overestimation" issue of MWR-retrieved LWP during raining periods, several examples are given in this appendix. We first calculated the extinction cross section per volume as a function of the drop equivolume diameter for the two frequencies in MWR (23.8 GHz and 31.4 GHZ) with a T-matrix method (Figure B). It is clearly shown that the extinction cross section increases with increased diameter when the diameters are smaller than 3 mm. This result reveals that the extinction (cross section) for rain drops (diameter > ~50 um) is much larger than that for cloud droplets (diameter < ~50 um). We also calculated the extinction coefficient as a function of RLWC for populations with three different drop size distributions (DSDs). The DSDs are modeled according to the exponential Marshall and Palmer (MP) distribution $N(D) = N_0 e^{-\Lambda D}$, where N_0=8000 m^{-3} mm^{-1}. N_0 is changed to 4000 and 32000 m^{-3} mm^{-1} to represent thunderstorm and drizzle DSDs. More details of the DSDs please see Battaglia et al. (2009). Figure C clearly shows the extinctions of cloud and rain also is DSD-dependent. For example, at 31.4 GHz, even though the RLWC is the same, the extinctions are much larger from the precipitation with the thunderstorms and MP DSDs than the extinctions from light precipitation with the drizzle DSD.

In addition, the brightness temperatures at 23.8 and 31.4 GHz channels are calculated using the MicroWave Radiative Transfer (MWRT) model. Five different sensitivity tests are generated with five combinations of CLWP and RLWP values (Table A). Table A lists the results and clearly demonstrates that the brightness temperatures in channels increase with increased cloud water amount (larger CLWP) and the rain water amount (larger RLWP). Comparing the results from test #2 and #3, it is clearly seen that the brightness temperatures contributed by rain drops are 31 and 51 K more than that contributed by cloud droplets at the frequencies of 23.8 and 31.4 GHz, even though their LWPs are the same (1 kg m^{-2}) in these two tests.

3)Also a key effect in enhancing brightness temperature is the presence of the melting layer (relevant literature must be cited).

Yes, Battaglia et al (2003) found the brightness temperature generally increases if mixed-phase precipitation is included.

In the revision, "The LWP differences between MWR retrieval and this study could be caused by the following reasons. 1) MWR-retrieved LWP represents the entire vertical

column (RWLP and CLWP below melting layer, large water coated ice particles in the melting layer and supercooled LWCs above the melting layer), while our retrieval only represents the LWP below the melting base. As Battaglia et al (2003) pointed out the brightness temperature generally increases if mixed-phase precipitation is included. 2) The MWR radome was wet during the raining periods and the deposition of raindrops on the radome can cause a large increase in the measured brightness temperatures (Cadeddu et al., 2017). 3) Large extinctions due to rain drops would affect MWR retrievals. 4) Uncertainties exist in the retrieved LWP from this study."

4)I found also the discussion at line 315-324 a bit confused: I am not sure why you want to include other disdrometers located within 5 km. I would suggest to delete it.

As suggested, we only include the comparison from the closed 2DVD and RD-80 with retrievals. The comparisons between measurements from other 2DVDs and the corresponding discussions are deleted.

5) Figure A: it would be good to see also contour lines with the values of mu.

As suggested, the contour lines with the miu values are added in the Figure A (b).

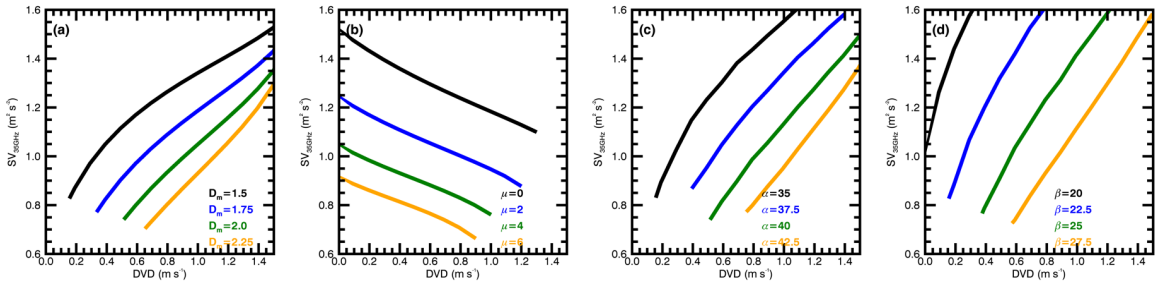

Figure A. Comparisons of (a) mass-weighted mean diameter D_m (mm), (b) shape parameter μ, (c) parameter α= 10 log(Z_{3GHz}/RLWC), and (d) parameter β = 10 log(Z_{3GHz}/RR) calculated as functions of Doppler velocity difference (DVD) and spectrum variance at 35 GHz (SV_{35GHz}). Note that the units of RLWC and RR are g m^{-3} and mm hr^{-1}.

6) Several typos (e.g. line 196, 292)

Thanks for the carefully check. The typos are corrected.

7) The names of the parameters in the Appendix are not optimal, e.g. Z_3GHz RR does not suggest a ratio. Also their units is not dB as stated in the caption of Fig.1. (dB corresponds to 10 log10 of a UNITLESS quantity!!!); here you are defining a very specific unit (like the dBZ, you need to specify the units used for z and LWC).

Variable names are changed.

In the revision, the variables are defined as α and β

$$\alpha = 10 \log_{10}(Z_{DSD}^{3GHz}/RLWC) \quad \textbf{(A11)}$$

$$\beta = 10 \log_{10}(Z_{DSD}^{3GHz}/RR) \quad \textbf{(A12)}$$

The review's comments are right, the units of α and β should not be dB.
Instead of defining the units of α and β, as suggested, the units of RLWC and rain rate are specified in the captions of Figure A.

Estimation of Liquid Water Path below the Melting Layer in Stratiform Precipitation Systems using Radar Measurements during MC3E

Jingjing Tian[1], Xiquan Dong[1], Baike Xi[1], Christopher R. Williams[2], and Peng Wu[1]

[1]Department of Hydrology and Atmospheric Sciences, University of Arizona, Tucson, Arizona, USA

[2] Department of Ann and H.J. Smead Aerospace Engineering Sciences, University of Colorado Boulder

Manuscript Submitted to Atmospheric Measurement Techniques

Corresponding author address: Dr. Xiquan Dong, The Department of Hydrology and Atmospheric Sciences, University of Arizona, 1133 E. James Rogers Way, Tucson, AZ 85721-0011.

Email: xdong@email.arizona.edu; Phone: 520-621-4652

Abstract

In this study, the liquid water path (LWP) below the melting layer in stratiform precipitation systems is retrieved, which is a combination of rain liquid water path (RLWP) and cloud liquid water path (CLWP). The retrieval algorithm uses measurements from the vertically pointing radars (VPRs) at 35 GHz and 3 GHz operated by the U.S Department of Energy Atmospheric Radiation Measurement (ARM) and National Oceanic and Atmospheric Administration (NOAA) during the field campaign Midlatitude Continental Convective Clouds Experiment (MC3E). The measured radar reflectivity and mean Doppler velocity from both VPRs and spectrum width from the 35 GHz radar are utilized. With the aid of the cloud base detected by ceilometer, the LWP in the liquid layer is retrieved under two different situations: (I) no cloud exists below the melting base, and (II) cloud exists below the melting base. In (I), LWP is primarily contributed from raindrops only, i.e., RLWP, which is estimated by analyzing the Doppler velocity differences between two VPRs. In (II), cloud particles and raindrops coexist below the melting base. The CLWP is estimated using a modified attenuation-based algorithm. Two stratiform precipitation cases (20 May 2011 and 11 May 2011) during MC3E are illustrated for two situations, respectively. With a total of 13 hours of samples during MC3E, statistical results show that the occurrence of cloud particles below the melting base is low (9%), however, the mean CLWP value can be up to 0.56 kg m^{-2}, which is much larger than the RLWP (0.10 kg m^{-2}). When only raindrops exist below the melting base, the averaged RLWP value is larger (0.32 kg m^{-2}) than the with cloud situation. The overall mean LWP below the melting base is 0.34 kg m^{-2} for stratiform systems during MC3E.

1. Introduction

Clouds in stratiform precipitation systems are important to the Earth's radiation budget. The vertical distributions of cloud microphysics, ice and liquid water content (IWC/LWC), determine the surface and top-of-the-atmosphere radiation budget and redistribute energy in the atmosphere (Feng et al., 2011; 2018). Also, stratiform precipitation systems are responsible for most tropical and midlatitude precipitation during summer (Xu, 2013). However, the representation of those systems in global climate and cloud-resolving models is still challenging (Fan et al., 2015). One of the challenges is due to the lack of comprehensive observations and retrievals of cloud microphysics (e.g. prognostic variables IWC and LWC) in stratiform precipitation systems. Liquid water path (LWP), defined as an integral of LWC in the atmosphere. It is a parameter used to provide the characterization of liquid hydrometeors in the vertical column of atmosphere and study clouds and precipitation. The estimation of LWC/LWP is one of the critical objectives of the US Department of Energy's (DOE) Atmospheric Radiation Measurement (ARM) Program (Ackerman and Stokes, 2003).

LWP can be retrieved using the ground-based MicroWave Radiometer (MWR) sensed downwelling radiant energy at 23.8 and 31.4 GHz (Liljegreen et al., 2001). In last two decades, ARM has been operating a network of 2-channel (23.8- and 31.4-GHz) ground-based MWR to provide a time series of LWP at the ARM Southern Great Plains (SGP) site (Cadeddu et al., 2013). Absorption-based algorithms using multichannels of MWRs have been widely used to retrieve cloud LWP (e.g., Liljegren et al. 2001; Turner, 2007), and they are known to be accurate methods to estimate LWP of nonprecipitating clouds with mean LWP error of 15 g m^{-2} (Crewell and Löhnert, 2003). However, in precipitating conditions, LWP retrieved from conventional

66 MWR are generally not valid due to the violation of the Rayleigh assumption when large
67 raindrops exist (e.g., Saavedra et al., 2012). In addition, large increase of brightness
68 temperatures is measured as a result of the deposition of raindrops on the MWR's radome.
69 Unfortunately, it is very hard to model and quantify this increase from rain layer on the radome
70 (Cadeddu et al., 2017). This "wet-radome" issue largely inhibits the retrieving of LWPs using
71 ground-based MWR during precipitation. Due to the limitations of retrieving LWP from MWR
72 during precipitation, cloud and precipitation radars were used to simultaneously retrieve LWP
73 (Matrosov, 2010).

74 In the precipitating system, the liquid water cloud droplets and raindrops often coexist in
75 the same atmospheric layer (e.g., Dubrovina, 1982; Mazin, 1989; Matrosov, 2009, 2010),
76 indicating that the LWP consists of both cloud liquid water path (CLWP) and rain liquid water
77 path (RLWP). However, the discrimination between suspended small cloud liquid water droplets
78 and precipitating large raindrops is a very challenging remote sensing problem. Even though the
79 partitioning of LWP into CLWP and RLWP is important in cloud modeling (Wentz and Spencer,
80 1998; Hillburn and Wentz, 2008), there are few studies retrieved RLWP and CLWP
81 simultaneously and separately (Saavedra et al., 2012; Cadeddu et al., 2017). Battaglia et al.
82 (2009) developed an algorithm to retrieve RLWP and CLWP from the six Advanced Microwave
83 Radiometer for Rain Identification (ADMIRARI) observables under rainy conditions. Saavedra
84 et al (2012) developed an algorithm using both ADMIRARI and a micro rain radar to retrieve
85 and analyze the CLWP and RLWP for midlatitude precipitation during fall. In addition to these
86 RLWP and CLWP estimations mainly from passive microwave radiometers, there are several
87 studies to estimate the LWP using active radar measurements only. Ellis and Vivekanandan
88 (2011) developed an attenuation-based technique to estimate LWC, which is the sum of cloud

89 water contents (CLWC) and rain liquid water contents (RLWC), using simultaneous S- and Ka-
90 band scanning radars measurements. However, it is not always applicable of using these
91 techniques to retrieve LWC. If raindrop diameters are comparable to at least one of the radars'
92 wavelength, "Mie effect" will be included in the measured differential reflectivity, however this
93 "Mie effect" is not very distinguishable from differential attenuation effects (Tridon et al., 2013;
94 Tridon and Battaglia 2015).

95 Matrosov (2009) developed an algorithm to simultaneously retrieve CLWP and layer-
96 mean rain rate using the radar reflectivity measurements from three ground-based W-, Ka-, S-
97 bands radars. The CLWP were retrieved based on estimating the attenuation of cloud radar
98 signals compared to S-band radar measurements. Matrosov (2010) developed an algorithm to
99 estimate CLWP using a vertical pointing Ka-band radar and a nearby scanning C-band radar.
100 The layer-mean rain rate was first estimated with the aid of surface disdrometer, and then CLWP
101 was retrieved by subtracting the rain attenuation from total attenuation measured from two radars.
102 For the estimation of RLWP, Williams et al. (2016) developed a retrieval algorithm for rain drop
103 size distribution (DSD) using doppler spectrum moments observed from two collocated vertical
104 pointing radar (VPRs) at frequencies of 3 GHz and 35 GHz. The retrieved air motion and DSD
105 parameters were evaluated using the retrievals from a collocated 448-MHz VPR.

106 In this study, the CLWP retrieval algorithms in Matrosov (2009 and 2010) have been
107 modified given the available radar measurements, vertical pointing Ka- and S-band radars,
108 during the Midlatitude Continental Convective Clouds Experiment (MC3E) field campaign. For
109 the estimation of RLWP, we will basically follow the idea described in Williams et al. (2016) to
110 retrieve microphysical properties for raindrops. However instead of retrieving vertical air
111 motion and rain DSDs (Williams et al., 2016), this study aims at retrieving RLWCs, and then

integrating RLWCs over the liquid layer to estimate RLWP. Overall, in this study, algorithms from three former publications are modified and combined to estimate the LWP in the stratiform precipitating systems.

The goals of this study are to retrieve the LWP below the melting base, which includes both RLWP and CLWP retrievals using radars measurements, and tentatively answer two questions based on observations and retrievals in the stratiform precipitation systems during MC3E: (1) what is the occurrence of cloud below the melting base in the stratiform precipitation systems; (2) what are the values of simultaneous CLWP, RLWP and LWP, and how does CLWP or RLWP contribute to the LWP. Note that the CLWP and RLWP are constrained in a stratiform precipitation layer below the melting base and above the surface. The LWP estimations in this study are primarily aimed at stratiform precipitating events exhibiting melting-layer features from radar measurements with lower-to-moderate rain rates (RR < 10 mm hr^{-1}). The instruments and data used in this study are introduced in section 2. Section 3 describes the methods of retrieving LWP (both RLWP and CLWP). Section 4 illustrates two examples and followed by statistical results from more samples during MC3E. The last section gives the summary and conclusions. Acronyms and abbreviations are listed in Table 1.

2. Data

The MC3E field campaign, co-sponsored by the NASA Global Precipitation Measurement and the U.S. DOE ARM programs, was conducted at the ARM SGP (northern Oklahoma) during April-June 2011 to study convective clouds and improve model parametrization (Jensen et al., 2015). MC3E provided an opportunity to develop new retrieval methods to estimate cloud microphysics and precipitation properties in precipitation systems

(Giangrande et al., 2014; Williams, 2016; Tian et al., 2016; Tian et al, 2018). Several stratiform rain cases were observed by the VPRs during MC3E (as shown in Fig. 1). Distinct signatures of "bright band" are detected from VPRs. To retrieve LWP associated with stratiform precipitation, this study mainly uses the observations from two co-located VPRs operating at 3-GHz and 35-GHz at DOE ARM SGP Climate Research Facility.

2.1 Vertical Pointing Radars

The 3-GHz (S-band) VPR was deployed by NOAA Earth System Research Laboratory for the six-weeks during the MC3E. The NOAA 3-GHz VPR is a vertical pointing radar with 2.6° beamwidth monitoring precipitation overhead. This 3-GHz profiler bridges the gap between cloud radars, which are used to provide the structure of nonprecipitating clouds but are severely attenuated by rainfall, and precipitation radars, which, although unattenuated by rainfall, generally lack the sensitivity to detect more detailed cloud structure. The 3-GHz VPR observes the raindrops within the Rayleigh scattering regime and its signal attenuation are negligible through the rain. The temporal resolution of the profiles of Doppler velocity spectra is 7 seconds and the vertical resolution is 60 meters. The 3-GHz VPR operated in two modes: a precipitation mode and a low-sensitivity mode. The precipitation mode observations are used in this study.

The Ka-band ARM zenith radar (KAZR) is also a vertical pointing radar, operating at 35 GHz permanently deployed by DOE ARM at the SGP site. The KAZR measurements include reflectivity, vertical velocity, and spectral width from near-ground to 20 km. The KAZR data used in this study are the KAZR Active Remote Sensing of Clouds (ARSCL) product produced by the ARM (www.arm.gov). The KAZR-ARSCL corrects for atmospheric gases attenuation and velocity aliasing. By selecting the mode with the highest signal-to-noise ratio at a given point, data from two simultaneous operating modes (general and cirrus mode) are combined for

each profile to provide the "best estimates" of radar moments in the time-height fields. The vertical and temporal resolutions of KAZR-ARSCL product are 30 meters and 4 seconds, respectively. Since the 3-GHz and 35-GHz VPRs are independent radars with different dwell time and sample volumes (Williams et al., 2016), the radar observations are processed to 1-min temporal and 60-m vertical resolutions in this study.

2.2 Disdrometers

DOE ARM program maintains a suite of surface precipitation disdrometers. Measurements and estimations from the Distromet model RD-80 disdrometer and NASA two-dimensional video disdrometers (2DVD) deployed at the ARM SGP site are used in this study. The RD-80 disdrometer provides the most continuous raindrop size distribution (DSD) measurements at high spectral (20 size bins from 0.3 to 5.4 mm) and temporal resolutions (1 minute), and its minimal detectable precipitation amount is 0.006 mm hr^{-1}. From 2DVD, the rain DSDs are observed from 41 bins (0.1 - 10 mm), and its minimal detectable precipitation amount is 0.01 mm hr^{-1}. In addition to rain rate, the mean mass-weighted raindrop diameter (D_m) is also provided from 2DVD, which is used for evaluating retrieved D_m from radar measurements.

2.3 Ceilometer

A Vaisala laser ceilometer (CEIL) operates at the SGP Central Facility, sensing cloud presence up to a height of 7700m with 10-m vertical resolution. The laser ceilometer transmits near-infrared pulses of light, and the receiver detects the light scattered back by clouds and precipitation. It is designed to measure cloud-base height.

3. The Methodology of Liquid Water Path Estimation

As mentioned earlier, both RLWP and CLWP contribute to the LWP. With the aid of the cloud base height detected by ceilometer, LWP is retrieved under two different situations: (I) the cloud base is higher than the melting base and (II) the cloud base is lower than the melting base. For situation (I), there are almost no cloud droplets below melting base (CLWP = 0), and thus the LWP below the melting base is solely from raindrops. The LWP is calculated by integrating RLWCs over this layer. The RLWCs could be retrieved by analyzing the measured Doppler Velocity Differences ("*DVD Algorithm*") from two collocated VPRs. In situation (II), the small cloud droplets and large raindrops coexist below the melting base. Both raindrops and cloud particles contribute to LWP. RLWP will be still estimated using "*DVD Algorithm*". CLWP will be retrieved using an attenuation-based algorithm named as "*Attenuation Algorithm*". The algorithms for LWP estimation are summarized in a flowchart (Fig. 2).

3.1 Situation I (no cloud droplets exist below the melting base)

The algorithm from Williams et al. (2016) was developed based on an assumption that the 3-GHz VPR operates within the Rayleigh scattering regime for all raindrops, while the 35-GHz VPR operates within the Rayleigh scattering regime for small raindrops (diameters < ~1.3 mm) and non-Rayleigh scattering regime for larger raindrops (diameters ≥ ~1.3 mm). The different scattering regimes for the two operating frequencies result in different estimated radar moments. These estimated radar moments are in functions of rain microphysics. Thus, the rain microphysics could be retrieved with given measured radar moments. The details of this "*DVD Algorithm*" and uncertainty estimation are introduced in Appendix A.

3.2 Situation II (cloud particles and rain droplets coexist below the melting base)

In situation (II), substantial cloud particles exist below melting base, and both RLWP and CLWP retrievals are needed to estimate the LWP. The total two-way attenuation of 35-GHz

VPR signals, A (in decibels, dB), in a layer between the melting base and the cloud base, mainly consists of rain attenuation, liquid clouds attenuation, and gaseous attenuation. The total attenuation (A) are expressed as:

$$A = 2\,C\,R_m\,\Delta H + 2\,B\,CLWP + G. \quad (1)$$

R_m is layer-mean rain rate, and ΔH (km) is the thickness of the layer (Matrosov, 2009). G is the two-way attenuation/absorption from atmospheric gases, which is relatively small, and the absorption by gases has been already corrected in the KAZR ARSCL dataset and is assumed to be zero in our retrieval.

C and B are the coefficients for rainfall and cloud liquid water attenuation.

$$B = 0.0026\pi\lambda^{-1}\mathrm{Im}[-(m^2-1)(m^2+2)^{-1}], \quad (2)$$

where λ is the wavelength of Ka-band radar, and m is the complex refractive index of water. The unit of B is dB/g m^{-2}.

$$C = 0.27\,b, \quad (3)$$

where b is the correction factor considering raindrop fall velocities with changing air density.

$$b = (\rho_{am}/\rho_{a0})^{0.45}, \quad (4)$$

where ρ_{am} and ρ_{a0} are the mean air density in the rain layer and the density at normal atmospheric conditions.

Based on (1), CLWP can be written as:

$$CLWP = \frac{A - 2\,C\,R_m\,\Delta H - G}{2\,B} \quad (5)$$

The attenuation (A) is estimated by comparing the drop in Ka-band reflectivity with the un-attenuated S-band reflectivity through the cloud. Assuming the changes in reflectivity with altitude due to changes in raindrop size distributions with altitude are similar for Ka- and S-band

reflectivities, then the difference in reflectivities through the cloud is a proxy for attenuation. This can be expressed using

$$A \cong [Z_{Ka}(cloud\ base) - Z_{Ka}(melting\ base)] - [Z_S(cloud\ base) - Z_S(melting\ base)] \quad (6)$$

Notice that the absolute calibration of the radar was not important to the retrieval results since the retrieval of CLWP used S-Ka differential attenuation. This avoids the radar calibration (Tridon et al., 2015 and 2017), which is a serious issue limiting the accuracy of radar retrievals.

The R_m is estimated as:

$$R_m = \frac{\sum_{h0}^{MB} RR(h) \times \Delta h}{\Delta H}, \quad (7)$$

where Δh equals 60 meters and MB is the melting base and h_0 is the height of the lowest unsaturated KAZR rang gate (Matrosov, 2010). RRs in the layer between the melting base and the cloud base are calculated from the "*DVD algorithm*".

The uncertainties of retrieved CLWP are mainly due to the uncertainties of estimated R_m and observed total attenuation from VPRs. The value of B is on the order of 1 dB/kg m^{-2}. The uncertainty of retrieved CLWP would be ~ 0.25 kg m^{-2} with 0.5 dB uncertainty from measured radar reflectivity difference or ~ 0.5 kg m^{-2} for 1.0 mm hr^{-1} uncertainty from estimated layer-mean rain rate. Compared to the typical mean rain rate observed in the stratiform system (~ 2 - 4 mm hr^{-1}), 1.0 mm hr^{-1} represents a ~ 30% uncertainty. The uncertainty for CLWP retrievals is roughly estimated as ~ 0.56 kg m^{-2} (sqrt (0.25^2+0.5^2)) in this study. For reference, the expected uncertainty is reported as ~ 0.25 kg m^{-2} for typical rainfall rates (~ 3 - 4 mm hr^{-1}) in Matrosov (2009) retrieval method. More details of the estimation of CLWP uncertainties are in Appendix B.

4. Retrieval Results and Discussions

4.1 Case Studies

Even though situation (I) is dominated (Fig. 1), especially in Case A, the ceilometer cloud base estimates can be lower than the melting base (Cases B to D). Two case studies (20 May 2011 and 11 May 2011) are given as examples to demonstrate the estimation of LWP in stratiform precipitation system for two different situations.

4.1.1 Case A

On 20 May 2011, an upper level low-pressure system at central Great Basin moved into the central and northern Plains, while a surface low pressure at southeastern Colorado brought the warm and moist air from the southern Plains to a warm front over Kansas. and a dry line extended southward from the Texas-Oklahoma. With those favorable conditions, a strong north-south oriented squall line developed over Great Plains and propagated eastward. The convection along the leading edge of this intense squall line exited the ARM SGP network around 11 UTC 20 May leaving behind a large area of stratiform rain (Case A in Fig. 1). This stratiform system passed over the ARM SGP site and observed by two VPRs, and disdrometers as shown in Figures 1a-1c. It clearly shows the 3-GHz radar echo tops are much lower than those from the 35 GHz VPR. Even though there is attenuation at 35-GHz by the raindrops and melting hydrometeors, the 35-GHz radar can still detect more small ice particles at near the cloud top. The “bright band”, which occurs in a uniform stratiform rain region, is clearly seen from the 3-GHz VPR (a sudden increase and then decrease in radar reflectivity) but is not obvious from the 35-GHz VPR due to the non-Rayleigh scattering effects at 35 GHz (Sassen et al., 2005; Matrosov, 2008).

Figures 1a-1b clearly show that the ceilometer detected cloud base is in the middle of the melting layer, indicating almost no cloud particles below the melting layer and the LWP in the liquid layer equals to RLWP. The RLWP is retrieved using the “*DVD Algorithm*” introduced in

271 section 3.1 and Appendix A. Figure 3 shows an example of the DVD retrieval algorithm at
272 13:40 UTC on May 20, 2011. Radar reflectivity from 3 GHz, Doppler velocities from 3 GHz
273 and 35 GHz, and spectrum variance from 35 GHz are the inputs of DVD algorithm. The
274 Doppler velocity differences (3 GHz – 35 GHz) from the surface to 4 km are also plotted in Fig.
275 3d. The melting base is defined as the height of maximum curvature in the radar reflectivity
276 profile at 3 GHz (Fabry and Zawadzki, 1995), which is clearly seen at 2.5 km in Fig. 3. Below
277 2.5 km, the Doppler velocity differences between the two VPRs become relatively uniform,
278 indicating that the process of melting snow/ice particles into raindrops is completed. Retrieved
279 profiles of rain microphysical properties and their corresponding uncertainties (horizontal bars at
280 different levels) in the rain layer (0 – 2.5 km) are shown in Figs 3f-3h. In general, the retrieved
281 D_m values from the surface to 2.5 km are nearly a constant of ~2 mm (Fig. 3f), while the
282 retrieved RLWC and rain rate values slightly decrease from 2.5 km to the surface. One of the
283 highlights of this study is, in addition to the surface rain rate, which can usually be observed
284 using surface disdrometers, the vertical profiles of rain microphysical properties are retrieved.
285 These retrieved rain microphysical properties will shed light on the understanding of liquid cloud
286 and rain microphysical processes (like condensation, evaporation, autoconversion and accretion
287 etc.) in the models.

288 To evaluate the rain property retrievals, we compare the retrieved rain microphysical
289 properties, the D_m, and rain rate at the surface, with the surface disdrometers measurements (Fig.
290 4). The D_m values range from 1.0 to 2.5 mm during a 3.5-hr period with nearly identical mean
291 values of 1.79 mm and 1.81 mm from both retrievals and 2DVD measurements. There are large
292 variations for rain rates, ranging from 0 to 8 mm hr^{-1}, with means of 3.19, 3.17 and 2.88 mm hr^{-1},
293 respectively, from 2DVD, RD-80 and radar retrieval. The mean rain rates from 2DVD and RD-

80 measurements are almost the same although there are relatively large differences during certain time periods, while the retrievals from this study, on average, underestimate the rain rate by ~10% compared to the disdrometer measurements. More statistics (mean differences, their 95% confidence intervals of mean differences and root mean square errors) can be found in Table 2. Overall, the mean differences are within the retrieval uncertainties. The variation of RLWP (Fig. 4c) mimics the variation of retrieved rain rate in Fig. 4d. The mean value of RLWP is 0.55 kg m^{-2} for this case, which is also the LWP below the melting base.

4.1.2 Case B

On 11 May 2011, a surface cold front moved across the Oklahoma-Texas area and then convections were initiated. At 1600 UTC, a mesoscale convective system organized with a parallel stratiform precipitation region. Two-three hours later (~1830 UTC), the mesoscale convective system was transitioned to a trailing stratiform mode passed over the ARM SGP site. The large stratiform regions are observed by two VPRs and disdrometers as shown in Figs 1d-1f. Figures 1d-1f clearly show that the ceilometer detected cloud bases are lower than the melting bases occasionally. Under this situation, both RLWP and CLWP could contribute to the LWP below the melting base.

Firstly, the surface rain microphysics (D_m, RLWC, rain rate and RLWP) are retrieved using "*DVD Algorithm*". These rain property retrievals are compared with the surface disdrometers measurements (Fig. 5). The D_m values at the surface range from 0.90 to 2.30 mm during a 4.5-hr period with the mean values of 1.41 mm and 1.52 mm, respectively, from both retrievals and 2DVD measurements. The difference between the retrieval and 2DVD measurement may be due to different sampling volumes between radar and the surface disdrometer, as well as wind shear. The rain rates, in this case, vary quite large, ranging from

317 0.02 to 4.78 mm hr^{-1} with means of 1.36, 1.26 and 1.66 mm hr^{-1}, respectively from single 2DVD,
318 RD-80, and our retrieval. It is found that, from both Case A and Case B, the mean value from
319 RD-80 is smaller than that from 2DVD. This may be due to the different ranges of measurable
320 drop sizes from two types of disdrometers (0.3 - 5.4 mm for RD 80, while 0.1 to 10 mm for
321 2DVD). More statistics can be also found in Table 2. Overall, the mean differences are still
322 within the retrieval uncertainties for this case.

323 Secondly, the CLWP is retrieved using "Attenuation Algorithm" introduced in section
324 3.2. Figure 5c shows the time series of RLWP, CLWP and LWP retrievals. It is found that the
325 CLWP values (when they exist) are usually larger than RLWP values in the same vertical
326 column. When cloud droplets and raindrops coexist below the melting base, the mean values are
327 0.11 kg m^{-2} and 1.64 kg m^{-2} for RLWP and CLWP, and the corresponding LWP below the
328 melting layer is 0.76 kg m^{-2}. While when only raindrops exist below the melting base, there is no
329 CLWP (CLWP =0), and the RLWP and LWP are the same (with average of 0.34 kg m^{-2}). It is
330 noticed that even though the occurrence of CLWP is low (11%) in this case, the value of CLWP
331 can be very large when it exists, and it is about two times larger than the mean RLWP. The
332 mean value of LWP is 0.37 kg m^{-2} for all the samples in Fig. 5c. The blue uncertainty bars in
333 Figure 5c show the retrieved CLWP uncertainty with assuming both of the uncertainties of
334 attenuation and total rain rate are 30% (Ua=Ur=30%). Due to the variations of the attenuation
335 and total rain rate with time, the estimated uncertainties of CLWP varies point to point. More
336 details about the estimation of CLWP are in Appendix B.
337
338 **4.2 Statistical Results**

339 Box and whisker plots of retrieved RLWP, CLWP and LWP for situations (I), (II) and all
340 samples during MC3E are shown in Fig. 6. The horizontal orange and red dashed lines indicate
341 the median and mean, boundaries of the box represent the first and third quartiles, and the
342 whiskers are the 10^{th}- and 90^{th} -percentiles. During MC3E, a total of 13 hours of stratiform rain
343 were observed by VPRs at the ARM SGP Climate Research Facility, in which 91% and 9% the
344 samples are categorized into the situations (I) and (II), respectively. The mean RLWPs are 0.32
345 kg m^{-2} and 0.10 kg m^{-2} for the situations (I) and (II). There are a substantial amount of small
346 cloud droplets sustaining in the rain layer and having not yet converted to larger raindrops, which
347 may partially explain smaller RLWP in the situation (II). The mean value of surface rain rate is
348 2.06 mm hr^{-1} when cloud droplets exist, which is also smaller than the mean value (2.38 mm hr^{-1})
349 in the rain-only situation. The mean CLWP in the situation (II) is as large as ~0.56 kg m^{-2} even
350 though their occurrence is very low (9%), which is much larger than mean RLWP in the liquid
351 layer. The LWP from the situation (II) (0.66 kg m^{-2}) is much larger than the mean LWP from
352 the situation (I) (0.32 kg m^{-2}), which is primarily contributed by cloud droplets. The overall
353 mean LWP for stratiform rain during MC3E is 0.34 kg m^{-2}.

354 We also processed the ARM MWR retrieved LWPs during MC3E and compared them
355 with our retrievals as illustrated in Fig. 7a. The corresponding LWP uncertainties are also
356 provided as the grey error bar for each retrieval with rain rate indicated by colors. It is notice
357 that the MWR has no LWP estimation when the rain rate is large. The MWR-retrieved LWPs
358 increase with increased rain rate, and much larger than the new LWP retrievals at high rate rates.
359 The newly retrieved LWPs weakly correlate with rain rates, and most values are less than 1.0 kg
360 m^{-2}, especially at high rain rates. The MWR retrieved LWPs increase with rain rate generally.
361 The increase of retrieved LWP with rain rate from MWR is possibly due to the “wet radome”

effect (Cadeddu et al., 2017). In addition to the issue from standing water on the radome, the extinctions due to raindrops also affect MWR retrievals. The extinction for rain is much larger than that for cloud (Sheppard, 1996), and thus, the small amount of rain water could enhance the measured brightness temperature significantly. More details of extinctions and brightness temperature calculations are shown in Appendix B. Statistical results of the retrieved LWPs from this study and MWR are averaged for each measured rain rate bins (bin size = 0.25 mm hr^{-1}). The differences of LWPs from MWR and this study are shown in Fig. 7b. The LWP differences increase with increased rain rate. The LWP differences between MWR retrieval and this study could be caused by the following reasons. 1) MWR-retrieved LWP represents the entire vertical column (RWLP and CLWP below melting layer, large water coated ice particles in the melting layer and supercooled LWCs above the melting layer), while our retrieval only represents the LWP below the melting base. As Battaglia et al (2003) pointed out the brightness temperature generally increases if mixed-phase precipitation is included. 2) The MWR radome was wet during the raining periods and the deposition of raindrops on the radome can cause a large increase in the measured brightness temperatures (Cadeddu et al., 2017). 3) Large extinctions due to rain drops would affect MWR retrievals. 4) Uncertainties exist in the retrieved LWP from this study.

5. Summary and Conclusions

LWP is a critical parameter for studying clouds, precipitation, and their life cycles. LWP can be retrieved from microwave radiometer measured brightness temperatures during cloudy and light precipitation conditions. However, MWR-retrieved LWPs are questionable under moderate and heavy precipitation conditions due to the “wet radome” and large extinction effects

caused by large raindrops. LWPs below the melting base in stratiform precipitation systems are estimated, which include both RLWP and CLWP. The measurements used in this study are mainly from two VPRs, 35-GHz from ARM and 3-GHz from NOAA during the MC3E field campaign.

In this study, the microphysical properties of raindrops, such as D_m, RLWC (and RLWP), and RR, are estimated following the method described in Williams et al. (2016) using measurements from co-located Ka- and S-band radars VPRs. The retrieved rain microphysical properties are validated by the surface disdrometer measurements. Instead of retrieving vertical air motion and rain DSDs (Williams et al., 2016), this study aims at retrieving RLWCs and then integrating RLWCs over the liquid layer to estimate RLWP. The CLWP is retrieved based on the modifications of the methods in Matrosov (2009 and 2010) with available radar measurements, vertical pointing Ka- and S-band VPRs, during the MC3E field campaign.

The applicability of retrieval methods is illustrated for two stratiform precipitation cases (20 May 2011 and 11 May 2011) observed during MC3E. Statistical results from a total of 13 hours samples during MC3E show that the occurrence of cloud droplets below the melting base is low (9%), while the CLWP value can be up to 0.56 kg m^{-2}, which is much larger than the RLWP (0.10 kg m^{-2}). When only raindrops exist below the melting base, the averaged RLWP value is 0.32 kg m^{-2}, which is much larger than the mean RLWP in the cloud droplets and raindrops coexisted situation.

Reliable retrievals of RLWC and RLWP are critical for model evaluation and improvement, as RLWC (rain mixing ratio) is an important prognostic variable in weather and climate models. Furthermore, the retrievals in the whole rain layer would be useful to understand the microphysical processes (i.e., condensation, evaporation, autoconversion, and

accretion etc.) and have great potential to improve model parametrizations in the future. Overall, the LWP (CLWP and RLWP) retrievals derived in this study can be used to evaluate the models that separately predict cloud and precipitation and contribute comprehensive information to study cloud-to-precipitation transitions.

Appendix A: Doppler Velocity Differences Algorithm ("*DVD Algorithm*")

Retrieving RLWC and other rain microphysical properties (i.e., drop size and rain rate) is based on the mathematics of DSD radar reflectivity-weighted velocity spectral density S_{DSD}^{λ} [(mm^6 m^{-3}) (m s^{-1})$^{-1}$], which is a product of radar raindrop backscattering cross section $\sigma_b^{\lambda}(D)$ (mm^2) and DSD number concentration $N_{DSD}(D)$ (mm^{-1} m^{-3}):

$$S_{DSD}^{\lambda}(v_z) = \left[\frac{\lambda^4}{\pi^5 |K_w|^2}\sigma_b^{\lambda}\right] N_{DSD}(D)\frac{dD}{dv_z}. \quad (A1)$$

The $\frac{dD}{dv_z}$ [mm (m s^{-1})$^{-1}$] is used as a coordinate transformation from diameter to velocity, where v_z (m s^{-1}) is the raindrop terminal velocity of diameter D (mm) at altitude z. λ is the wavelength of radar. $|K_w|^2$ equals 0.93 and it is the dielectric factor.

The $N_{DSD}(D)$ can be expressed as a normalized gamma shape distribution with three parameters (Leinonen et al., 2012):

$$N_{DSD}(D; N_w, D_m, \mu) = N_w f(D;\ D_m, \mu), \quad (A2)$$

where

$$f(D;\ D_m, \mu) = \frac{6}{4^4}\frac{(\mu+4)^{(\mu+4)}}{\Gamma(\mu+4)}\left(\frac{D}{D_m}\right)^{\mu}\exp\left[-(\mu+4)\frac{D}{D_m}\right]. \quad (A3)$$

N_w is the scaling parameter, μ is a shape parameter, $\Gamma(x)$ is the Euler gamma function, and D_m is a mean mass-weighted raindrop diameter estimated from the ratio of the fourth to third DSD moments:

$$D_m = \frac{M_4}{M_3} = \frac{\int_{D_{min}}^{D_{max}} N_{DSD}(D) D^4 dD}{\int_{D_{min}}^{D_{max}} N_{DSD}(D) D^3 dD}. \quad (A4)$$

where D_{min} and D_{max} represent the minimum and maximum diameters in the distribution, respectively.

The intrinsic (non-attenuation) reflectivity factor and the mean velocity and the spectrum variance are the zeroth, first, and second reflectivity-weighted velocity spectrum moments:

$$Z_{DSD}^{\lambda} = \sum_{v_{min}}^{v_{max}} S_{DSD}^{\lambda}(v_i) \Delta v \quad (A5)$$

$$v_{DSD}^{\lambda} = \frac{\sum_{v_{min}}^{v_{max}} S_{DSD}^{\lambda}(v_i)\, v_i\, \Delta v}{Z_{DSD}^{\lambda}} \quad (A6)$$

$$SV_{DSD}^{\lambda} = \frac{\sum_{v_{min}}^{v_{max}} (v_i - v_{DSD}^{\lambda})^2 S_{DSD}^{\lambda}(v_i)\, \Delta v}{Z_{DSD}^{\lambda}}. \quad (A7)$$

where v_i is the discrete velocities and Δv is velocity resolution in the integration.

The Doppler Velocity Difference (DVD) is defined as

$$DVD = v_{DSD}^{3\ GHz} - v_{DSD}^{35\ GHz}. \quad (A8)$$

Note that both DVD and SV are dependent on DSD parameters (D_m and μ) only.

The RLWC and rain rate (RR) can also be described using the DSD:

$$RLWC(g\ m^{-3}) = \frac{\pi}{6} 10^{-3} \sum_{D_{min}}^{D_{max}} N_{DSD}(D, N_w, D_m, \mu) D_i^3 \Delta D \quad (A9)$$

$$RR(mm\ hr^{-1}) = \frac{6\pi}{10^4} \sum_{D_{min}}^{D_{max}} N_{DSD}(D, N_w, D_m, \mu) D_i^3 v_z(D_i) \Delta D. \quad (A10)$$

In addition, there are two newly defined radar-related parameters (α and β), which are also dependent on D_m and μ only:

$$\alpha = 10 \log_{10}(Z_{DSD}^{3GHz}/RLWC) \quad (A11)$$

$$\beta = 10 \log_{10}(Z_{DSD}^{3GHz}/RR) \quad (A12)$$

In this study, four variables, DVD, SV at 35 GHz (SV_{35GHz}), α and β, are pre-calculated using different groups of D_m and μ values, and then these values are stored in look-up tables

(LUTs). Raindrop backscattering cross sections are calculated using the T-matrix with different temperatures and oblate raindrop axis ratios (Leinonen, 2014). LUT examples are illustrated in Fig. A as functions of DVD and SV_{35GHz}. If we assume that the observed radar Doppler velocity difference and spectrum variance from the 35-GHz radar is equal to the DSD velocity difference and variance (DVD and SV_{35GHz}), the measured Doppler velocity difference and spectrum variance at 35-GHz can determine a solution for D_m from the LUT (Fig. A(a)). Similarly, a value of Z_{3GHZ}LWC (or Z_{3GHZ}RR) can be found with measured DVD and SV_{35GHz} using the LUT in Fig. A(b) (or Fig. A(c)). Then RLWC (or RR) can be estimated using (A11) (or (A12)) with measured reflectivity at 3-GHz (Z_{3GHZ}).

The observed radar Doppler velocity difference can be assumed to be equal to the DSD velocity difference for two reasons: (1) even though the radar observed Doppler velocity spectrum can be broaden by the air motion, this spectrum broadening variance is small (within 2%) relative to the DSD velocity spectrum because of the narrow beamwidth (0.2^o) of KAZR and (2) spectrum broadening is symmetric, which does not affect the first spectrum moment and the DSD mean Doppler velocity only shifts due to the air motion. Therefore, the measured differences of Doppler velocity between the 3-GHz and 35- GHz radars vertical pointing observations are independent of air motion and can be assumed to be the same as DVD from (A8). The validity of such an assumption is fully discussed in Williams et al. (2016).

The variabilities of 3-GHz and 35-GHz VPR observations within each 1-minute/60-meter bin are regarded as the measurement uncertainties and will be propagated through the retrieval to produce retrieval uncertainties. The retrieval uncertainties are estimated follow two steps: (1) construct a distribution of input radar measurements. For example, the temporal resolution for 3-GHz VPR is seven seconds, thus there are about nine radar reflectivities observed for one minute.

474 A normal distribution is generated first using the mean and standard deviations of these nine
475 observed radar reflectivities for this 1-min/60-m resolution/bin. (2) repeat the DVD retrievals
476 using samplings from distributions of all input measurements. We randomly select 100 groups
477 of members from those (DVD, SV_{35GHz}, Z_{3GHZ}) normal distributions to form 100 realizations, and
478 then produce 100 separate output estimates. The mean and standard deviation of the 100
479 solutions are regarded as the final retrieval and the retrieval uncertainty.

480 The uncertainties of RLWP are estimated based on the uncertainties of RLWC. More
481 specifically, we first estimated the RLWC uncertainties at each height level, and then we
482 calculated the ratios of RLWC uncertainties to the mean retrieved RLWCs at each height level,
483 which represent percentage values of retrieval uncertainties. Finally, we calculated the mean
484 ratio of the uncertainties in the whole liquid layer below melting base and regarded this mean
485 ratio as the uncertainty of RLWP.

486 It is noted that the uncertainty here only considers estimates of instrument noise, not the
487 uncertainties associated with assumptions used in the retrieval. For example, the gamma size
488 distribution used in (A2) is an approximation which may introduce error into the retrieval.
489 However, it is very difficult to quantify this type of retrieval uncertainty. In this study, we
490 further compared our retrievals with independent surface disdrometers measurements to estimate
491 the uncertainties of retrievals. Also, when both radars are observing at Rayleigh scattering for
492 small raindrops, the reflectivity-weighted radial velocities for these particles should be the same.
493 In order to have a difference in radial velocity during the retrieval, large droplets must exist. The
494 maximum diameters in drop size distribution measured from disdrometer for all the stratiform
495 cases during MC3E are investigated. It is found that the occurrence of small-droplets-only
496 (maximum diameter <1.3 mm) is very low (less than 3%). Thus, it will not have a significant

497 impact on the retrieval results. Notice that this algorithm is not suitable for strong convective
498 rain due to the wind shear and strong turbulence as well as severe attenuation and extinction of
499 the Ka-band radar signal.
500
501 **Appendix B: CLWP Uncertainty**
502 CLWP can be simplified and estimated as following equation:

503 $$\mathrm{CLWP} = \frac{\mathrm{A} - 2\ \mathrm{C}\ R_{total}}{2\ \mathrm{B}}\ . \qquad \text{(B1)}$$

504 The attenuation (A) is estimated by comparing the drop in Ka-band reflectivity with the un-
505 attenuated S-band reflectivity. The rain attenuation is estimated by the rain attenuation
506 coefficient (C) multiplied by the total rain rate (R_{total}). C and B are the coefficients of rain and
507 cloud water attenuation with values of ~ 0.26 dB /km /mm hr^{-1} and ~ 0.87 dB / kg m^{-2},
508 respectively. The influence of temperature uncertainty in B on the retrieval error is minor
509 compared to the uncertainties of the total attenuation (A) and total rain rate (R_{total}) (Matrosov
510 2010). The uncertainty of CLWP is calculated as

511 $$\Delta \mathrm{C}LWP = \sqrt{(\frac{\partial CLWP}{\partial A} \times \Delta \mathrm{A})^2 + (\frac{\partial CLWP}{\partial R_{total}} \times \Delta R_{total})^2} \qquad \text{(B2)}$$

512 $$\Delta \mathrm{C}LWP = \sqrt{(\frac{1}{2B} \times \mathrm{A}\ \times \mathrm{Ua}\ )^2 + (-\frac{C}{B} \times R_{total} \times \mathrm{Ur}\ )^2} \qquad \text{(B3)}$$

513 For given uncertainties of attenuation (Ua) and total rain rate (Ur), the uncertainty of CLWP can
514 be calculated based on equation (B3).
515
516 **Appendix C: Calculations of Extinction and Brightness Temperature at Microwave**
517 **Radiometer Channels**

To better explain the "overestimation" issue of retrieved LWP from microwave radiometer, several examples are given in this appendix. Firstly, we calculated the extinction cross section per volume as a function of the drop equivolume diameter for the two frequencies in MWR (23.8 GHz and 31.4 GHZ) with a T-matrix method (Figure B). It is clearly shown that the extinction cross section is increasing with the diameter when the diameter is smaller than 3 mm. This indicates the extinction (cross section) for rain drops (diameter > ~ 50 um) is much larger than that for cloud droplets (diameter < ~50 um). Secondly, we calculated the extinction coefficient as a function of RLWC for populations with three different drop size distributions (DSDs). The DSDs are modeled according to the exponential Marshall and Palmer (MP) distribution $N(D) = N_0 e^{-\Lambda D}$, where N_0=8000 m^{-3} mm^{-1}. N_0 is changed to 4000 and 32000 m^{-3} mm^{-1} to represent thunderstorm and drizzle DSDs. More details of the DSDs please see Battaglia et al. (2009). Figure C clearly shows the extinctions of cloud and rain also is DSD-dependent. For example, at 31.4 GHz, even though the RLWC is the same, the extinctions are much larger from the precipitation with the thunderstorms and MP DSDs than the extinctions from light precipitation with the drizzle DSD.

In addition, the brightness temperatures at 23.8 and 31.4 GHz channels are calculated using the MicroWave Radiative Transfer (MWRT) model. Five different sensitivity tests are generated with five combinations of CLWP and RLWP values (Table A). Table A lists the results and clearly demonstrates that the brightness temperatures in channels increase with increased cloud water amount (larger CLWP) and the rain water amount (larger RLWP). Comparing the results from test #2 and #3, it is clearly seen that the brightness temperatures contributed by rain drops are 31 and 51 K more than that contributed by cloud droplets at the

frequencies of 23.8 and 31.4 GHz, even though their LWPs are the same (1 kg m^{-2}) in these two tests.

Acknowledgments: J. Tian and X. Dong are supported by DOE CMDV project under grant DE-SC0017015 at the University of Arizona, and B. Xi is supported by NASA CERES project under grant NNX17AC52G at the University of Arizona. C. R. Williams is supported by DOE ASR project under grant DE-SC0014294. Special thanks to Dr. Sergey Matrosov from NOAA Earth System Research Laboratory (ESRL) for his suggestions. Special thanks to Michael Jensen, PI of MC3E. Aircraft in situ measurements are processed using data from https://ghrc.nsstc.nasa.gov/pub/fieldCampaigns/gpmValidation/mc3e/, can also be obtained from Xiquan Dong (xdong@email.arizona.edu). NOAA vertical profile radar datasets are publically available in the DOE archives (http://iop.archive.arm.gov/arm-iop/2011/sgp/mc3e/williams-s_band/).

554 **References**

555 Ackerman, T. P., and Stokes, G. M: The Atmospheric Radiation Measurement Program. Phys.
556 Today, 56,38–44, doi:10.1063/1.1554135, 2003
557 Battaglia, A., Saavedra, P., T. Rose, and Simmer, C.: Characterization of precipitating clouds by
558 ground-based measurements with the triple-frequency polarized microwave radiometer
559 ADMIRARI, J. Appl. Meteorol., 49(3), 394–414, 2009
560 Battaglia, A., C. Kummerow, D. Shin, and C. Williams, 2003: Constraining Microwave
561 Brightness Temperatures by Radar Brightband Observations. J. Atmos. Oceanic
562 Technol., 20, 856-871, https://doi.org/10.1175/15200426(2003)020<0856:CMBTBR>2.0
563 .CO;2
564 Cadeddu, M. P., Liljegren, J. C., and Turner, D. D.: The Atmospheric radiation measurement
565 (ARM) program network of microwave radiometers: instrumentation, data, and retrievals,
566 Atmos. Meas. Tech., 6, 2359-2372, https://doi.org/10.5194/amt-6-2359-2013, 2013
567 Cadeddu, M. P., Marchand, R., Orlandi, E., Turner, D. D. and Mech, M. (2017). Microwave
568 Passive Ground-Based Retrievals of Cloud and Rain Liquid Water Path in Drizzling
569 Clouds: Challenges and Possibilities, IEEE Trans. Geosci. Remote Sens., vol. 55, no. 11,
570 pp. 6468-6481, doi: 10.1109/TGRS.2017.2728699
571 Crewell, S., and Löhnert, U. (2003). Accuracy of cloud liquid water path from ground-based
572 microwave radiometry 2. Sensor accuracy and synergy, Radio Sci., 38, 8042,
573 doi:10.1029/2002RS002634, 3.
574 Dubrovina, L. S.: Cloudness and precipitation according to the data of airplane soundings,
575 Gidrometeoizdat, Leningrad (in Russian), 218 pp,1982

576 Ellis, S. M., and Vivekanandan, J.: Liquid water content estimates using simultaneous S and K_a
577 band radar measurements, Radio Sci., 46, RS2021, doi:10.1029/2010RS004361, 2011
578 Fabry, F. and Zawadzki, I.: Long-Term Radar Observations of the Melting Layer of Precipitation
579 and Their Interpretation. J. Atmos. Sci., 52, 838–851, https://doi.org/10.1175/1520-
580 0469(1995)052<0838:LTROOT>2.0.CO;2, 1995
581 Fan, J., Liu, Y.-C., Xu, K.-M., North, K., Collis, S., Dong, X, and Ghan, S. J.: Improving
582 representation of convective transport for scale-aware parameterization:1. Convection
583 and cloud properties simulated with spectral bin and bulk microphysics, Journal of
584 Geophysical Research: Atmosphere, 120, 3485–3509,
585 https://doi.org/10.1002/2014JD022142, 2015
586 Feng, Z., Dong, X. Q., Xi, B. K., Schumacher, C., Minnis, P., and Khaiyer, M.: Top-of-
587 atmosphere radiation budget of convective core/stratiform rain and anvil clouds from
588 deep convective systems. Journal of Geophysical Research, 116, D23202. https://doi.org/
589 10.1029/2011JD016451, 2011
590 Feng, Z., Leung, L. R., Houze, R. A., Jr., Hagos, S., Hardin, J., Yang, Q., Han, B. and Fan, J.:
591 Structure and evolution of mesoscale convective systems: Sensitivity to cloud
592 microphysics in convection-permitting simulations over the United States. Journal of
593 Advances in Modeling Earth Systems, 10, 1470–1494.
594 https://doi.org/10.1029/2018MS001305, 2018
595 Giangrande, S. E., Collis, S., Theisen, A. K., and Tokay, A.: Precipitation estimation from the
596 ARM distributed radar network during the MC3E campaign, J. Appl. Meteor. Climatol.,
597 doi:10.1175/JAMC-D-13-0321.1, 2014

598 Jensen, M.P., Petersen, W. A., Bansemer, A., Bharadwaj, N., Carey, L. D., Cecil, D. J, and
599 Zipser, E. J.: The Midlatitude Continental Convective Clouds Experiment (MC3E),
600 Bulletin of the American Meteorological Society. 151221073208006.
601 https://doi.org/10.1175/BAMS-D-14-00228.1, 2015
602 Leinonen, J., Moisseev, D., M. Leskinen, M., and W.A. Petersen, W.A.: A Climatology of
603 Disdrometer Measurements of Rainfall in Finland over Five Years with Implications for
604 Global Radar Observations. J. Appl. Meteor. Climatol., 51, 392–404,
605 https://doi.org/10.1175/JAMC-D-11-056.1, 2012
606 Leinonen, J.: High-level interface to T-matrix scattering calculations: architecture, capabilities
607 and limitations, Opt. Express, vol. 22, issue 2, 1655-1660 doi: 10.1364/OE.22.001655,
608 2014
609 Liljegren, J. C., Clothiaux, E. E., Mace, G. G., Kato, S., and Dong, X.: A new retrieval for cloud
610 liquid water path using a ground-based microwave radiometer and measurements of
611 cloud temperature, J. Geophys. Res., 106(D13), 14485–14500,
612 doi:10.1029/2000JD900817, 2001
613 Lebsock, M.D., L'Ecuyer, T.S. and Stephens, G.L.: Detecting the Ratio of Rain and Cloud
614 Water in Low-Latitude Shallow Marine Clouds. J. Appl. Meteor. Climatol., 50, 419–432,
615 https://doi.org/10.1175/2010JAMC2494.1, 2011
616 Matrosov, S. Y.: Assessment of radar signal attenuation caused by the melting hydrometeor layer.
617 IEEE Trans. Geosci. Remote Sens., 46,1039–1047 doi: 10.1109/TGRS.2008.915757,
618 2008

619 Matrosov, S. Y.: A method to estimate vertically integrated amounts of cloud ice and liquid and
620 mean rain rate in stratiform precipitation from radar and auxiliary data, J. Appl. Meteor.
621 Climatol., 48, 1398–1410, doi:10.1175/2009JAMC2196.1, 2009
622 Matrosov, S. Y.: Synergetic use of millimeter- and centimeter-wavelength radars for retrievals of
623 cloud and rainfall parameters, Atmos. Chem. Phys., 10, 3321-3331,
624 https://doi.org/10.5194/acp-10-3321-2010, 2010
625 Mazin, I. P. (Ed.): Clouds and the Cloudy Atmosphere. Gidrometeoizdat, Leningrad, 648 pp,
626 1989.
627 Saavedra, P., Battaglia, A., and Simmer, C.: Partitioning of cloud water and rainwater content by
628 ground-based observations with the Advanced Microwave Radiometer for Rain
629 Identification (ADMIRARI) in synergy with a micro rain radar, J. Geophys. Res., 117,
630 D05203, doi:10.1029/2011JD016579, 2012
631 Sassen, K., Campbell, J. R., Zhu, J., Kollias, P., Shupe, M., and Williams, C.: Lidar and Triple-
632 Wavelength Doppler Radar Measurements of the Melting Layer: A Revised Model for
633 Dark- and Brightband Phenomena. J. Appl. Meteor., 44, 301–312,
634 https://doi.org/10.1175/JAM-2197.1, 2005
635 Sheppard, B.E.: Effect of Rain on Ground-Based Microwave Radiometric Measurements in the
636 20–90-GHz Range. *J. Atmos. Oceanic Technol.,* 13, 1139–1151,
637 https://doi.org/10.1175/1520-0426(1996)013<1139:EOROGB>2.0.CO;2, 1996
638 Tian, J., Dong, X., Xi, B., Wang, J., Homeyer, C. R., McFarquhar, G. M., and Fan J.: Retrievals
639 of ice cloud microphysical properties of deep convective systems using radar
640 measurements, Journal of Geophysical Research: Atmosphere., 121,10 ,820–10,839,
641 https://doi.org/10.1002/2015JD024686, 2016

642 Tian, J., Dong, X., Xi, B., Minnis, P., Smith, W. L., Jr, Sun-Mack, S., Thieman, M., Wang, J.:
643 Comparisons of ice water path in deep convective systems among ground-based, GOES,
644 and CERES-MODIS retrievals. Journal of Geophysical Research: Atmospheres, 123,
645 1708–1723. https://doi.org/10.1002/2017JD027498, 2018
646 Tridon, F., and Battaglia, A.: Dual-frequency radar Doppler spectral retrieval of rain drop size
647 distributions and entangled dynamics variables, J. Geophys. Res. Atmos., 120, 5585–
648 5601, doi:10.1002/2014JD023023, 2015
649 Tridon, F., Battaglia, A., and Kollias, P.: Disentangling Mie and attenuation effects in rain using
650 a Ka-W dual-wavelength Doppler spectral ratio technique, Geophys. Res. Lett., 40, 5548
651 5552, doi:10.1002/2013GL057454, 2013
652 Tridon, F., Battaglia, A., Luke, E., and Kollias, P.: Rain retrieval from dual-frequency radar
653 Doppler spectra: validation and potential for a 25 midlatitude precipitating case-study,
654 Quarterly Journal of the Royal Meteorological Society, 143, 1364–1380, 2017.
655 Turner, D. D., Clough, S. A., Liljegren, J. C., Clothiaux, E. E., Cady-Pereira, K. E., and Gaustad,
656 K. L.: Retrieving liquid water path and precipitable water vapor from the Atmospheric
657 Radiation Measurement (ARM) microwave radiometers. IEEE Trans. Geosci. Remote
658 Sens., 45, 3680–3690, 2007
659 Wentz, F.J. and Spencer, R.W.: SSM/I Rain Retrievals within a Unified All-Weather Ocean
660 Algorithm. J. Atmos. Sci., 55, 1613–1627, https://doi.org/10.1175/1520-
661 0469(1998)055<1613:SIRRWA>2.0.CO;2, 1998
662 Williams, C. R.: Reflectivity and liquid water content vertical decomposition diagrams to
663 diagnose vertical evolution of raindrop size distributions, J. Atmos. Oceanic Technol.,
664 doi:10.1175/JTECH-D-15-0208.1, 2016

665 Williams, C. R., Beauchamp, R. M., and Chandrasekar, V.: Vertical air motions and raindrop
666 size distributions estimated from mean Doppler velocity difference from 3- and 35-GHz
667 vertically pointing radars. IEEE Trans. Geosci. Remote Sens., 54, 6048–6060,
668 https://doi.org/10.1109/ TGRS.2016.2580526, 2016
669 Xu, W.: Precipitation and convective characteristics of summer deep convection over east Asia
670 observed by TRMM, Monthly Weather Review., 141, 1577-1592.
671 https://doi.org/10.1175/MWR-D-12-001

672
673 **Table 1**. Acronyms and Abbreviations Used in This Study

Acronyms and Abbreviations	Full Name
2DVD	Two-dimensional video disdrometer
A	Total two-way attenuation of 35-GHz VPR signals
ARSCL	Active remote sensing of clouds
ARM	Atmospheric Radiation Measurement
B	coefficients for cloud water attenuation
C	coefficients for rainfall attenuation
CLWP	Cloud liquid water path
D	Raindrop diameter
D_m	Mean mass-weighted raindrop diameter
D_{max}	Maximum diameters in the size distribution
D_{min}	Minimum diameters in the size distribution
DOE	Department of Energy
DSD	Drop size distribution
DVD	Doppler velocity difference
G	Two-way gaseous absorption
IWC	Ice water content
KAZR	Ka-band ARM zenith radar
LUT	Looking up table
LWP	Liquid water path
MB	Base of melting layer
MC3E	Mid-latitude continental convective clouds experiment
MMCR	Millimeter-wavelength cloud radar
MWR	Microwave radiometer
N_{DSD}	Number concentration
N_0	Intercept of ice particle size distribution
NOAA	National Oceanic and Atmospheric Administration
N_w	Scaling parameter in the drop size distribution
RLWP	Rain liquid water path
R_m	Layer-mean rain rate
RR	Rain rate

$\mathbf{S}_{\mathbf{DSD}}^{\boldsymbol{\lambda}}$	Radar reflectivity-weighted velocity spectral density
$\mathbf{v}_{\mathbf{DSD}}^{\boldsymbol{\lambda}}$	First reflectivity-weighted velocity spectrum moments represent the mean velocity
Vz	Raindrop terminal velocity
$\mathbf{Z}_{\mathbf{DSD}}^{\boldsymbol{\lambda}}$	Zeroth reflectivity-weighted velocity spectrum moments represent the intrinsic (non-attenuation) reflectivity factor
$\boldsymbol{\Gamma}(\mathbf{x})$	Euler gamma function
λ	Radar wavelength
$\boldsymbol{\sigma}_{\mathbf{b}}^{\boldsymbol{\lambda}}$	Raindrop backscattering cross section
μ	Shape parameter

674

675

676 **Table 2.** Statistics (mean differences, 95% confidence interval of mean differences, RMSEs) of D_m, RR between this study (RET) and
677 disdrometers (2DVD, RD-80) for Case A and Case B
678
679
680
681
682
683

	Mean Differences (95% confidence interval)	RMSE
Case A: D_m (RET, 2DVD) (mm)	0.04 (-0.07, -0.01)	0.24
Case A: RR (RET, RD-80) (mm hr^{-1})	-0.45 (-0.57, -0.33)	0.96
Case A: RR (RET, 2DVD) (mm hr^{-1})	-0.61(-0.77, -0.43)	1.38
Case B: D_m (RET, 2DVD) (mm)	0.10 (-0.14, -0.07)	0.27
Case B: RR (RET, RD-80) (mm hr^{-1})	0.40 (0.19, 0.60)	1.51
Case B: RR (RET, 2DVD) (mm hr^{-1})	0.30(0.09, 0.52)	1.58

684 **Table A.** The brightness temperatures (TB) at 23.8 and 31.4 GHz for different assumptions of CLWP and RLWP values.

Sensitivity Test	CLWP (kg m^{-2})	RLWP (kg m^{-2})	TB at 23.8 GHz	TB at 31.4 GHz
#1	2	0	197.20	196.28
#2	1	0	186.34	177.49
#3	0	1	217.28	228.20
#4	0	2	254.51	272.09
#5	1	1	225.37	239.88

685

686

687

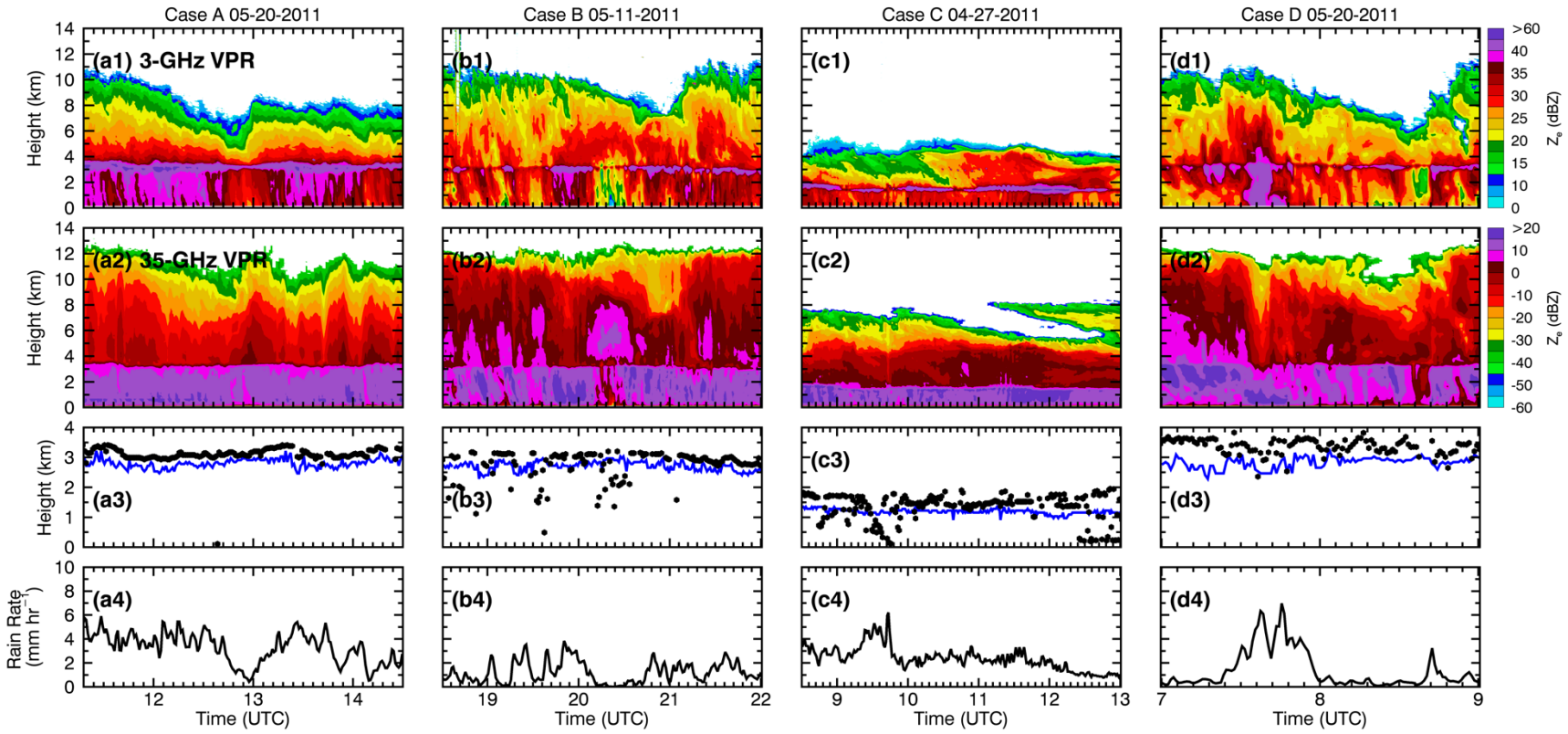

688

689 **Figure 1.** Time series of (a1) radar reflectivity (Z_e) from NOAA 3-GHz vertical pointing radar (VPR), (b1) radar reflectivity from
690 ARM 35-GHz VPR, (c1) melting base (blue lines) and cloud base (black dots), and (d1) rain rates from RD-80 surface disdrometer
691 measurement for Case A (20 May 2011, 11:20 – 14 :30 UTC); (b1)-(b4) for Case B (11 May 201, 18:30 – 22 :00 UTC); (c1)-(c4) for
692 Case C (27 April 2011, 8:30 – 13 :00 UTC); (d1)-(d4) for Case D (20 May 2011, 7:00 – 9 :00 UTC). Note that the ranges of radar
693 dBZ values are different in 3-GHz and 35-GHz radars.
694
695

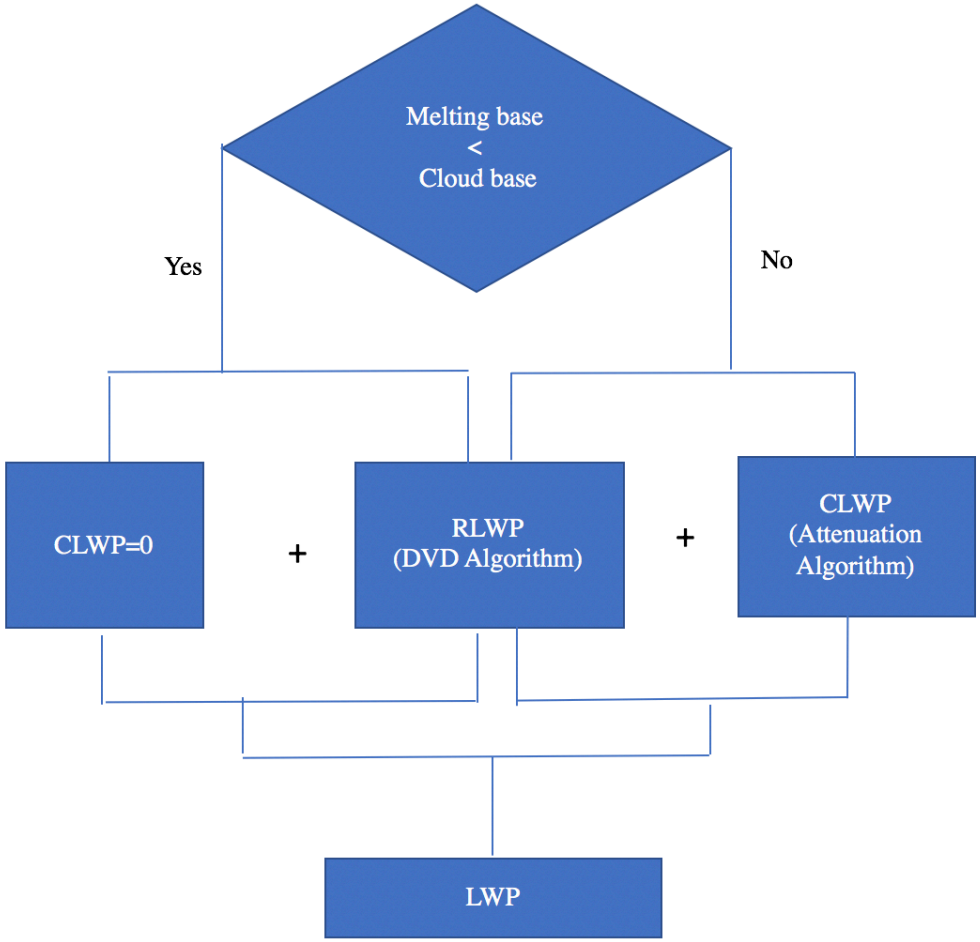

696

697 **Figure 2**. Algorithm flowchart to retrieve liquid water path (LWP) below melting base.

698

699

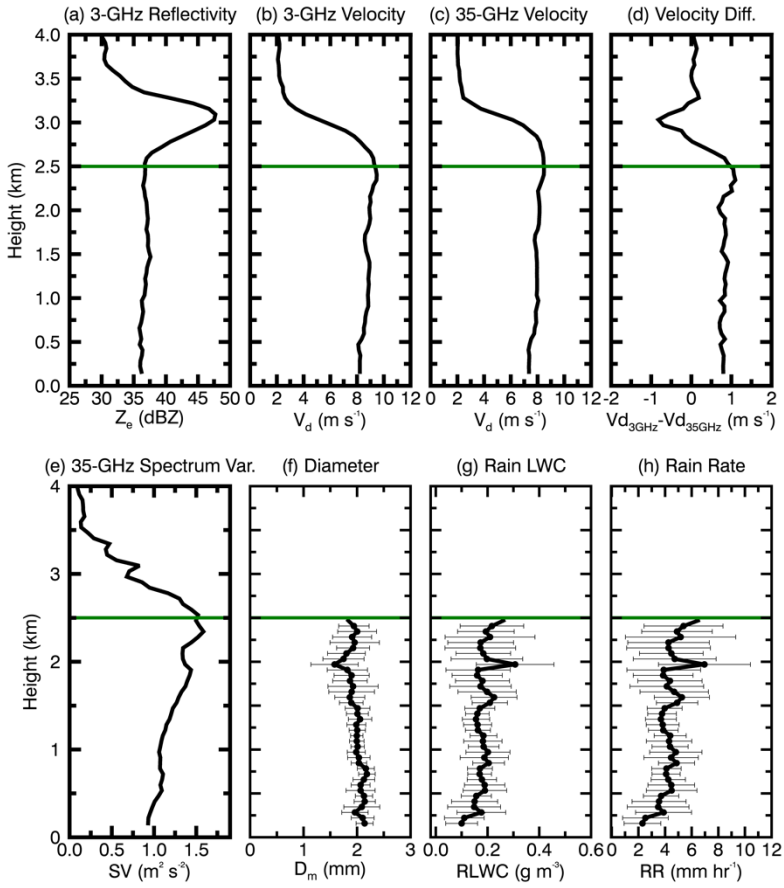

700

701 **Figure 3**. An example of illustrating the Doppler Velocity Differences (DVD) retrieval
702 algorithm at 13:40 UTC on May 20, 2011. The inputs of the DVD retrieval algorithm are: (a) 3-
703 GHz vertical pointing radar reflectivity factor (Z_e), (b) 3-GHz radar Doppler velocities (V_d), (c)
704 35-GHz radar Doppler velocities (V_d), and (e) 35-GHz radar spectrum variances (SV). The
705 Doppler velocity difference between 3-GHz and 35 GHz is shown in (d). The outputs of the
706 DVD retrieval algorithm are: (f) mass-weighted mean diameter D_m, (g) rain liquid water content
707 (RLWC), and (h) rain rate (RR). Retrieval uncertainties are shown as horizontal thin black lines.
708

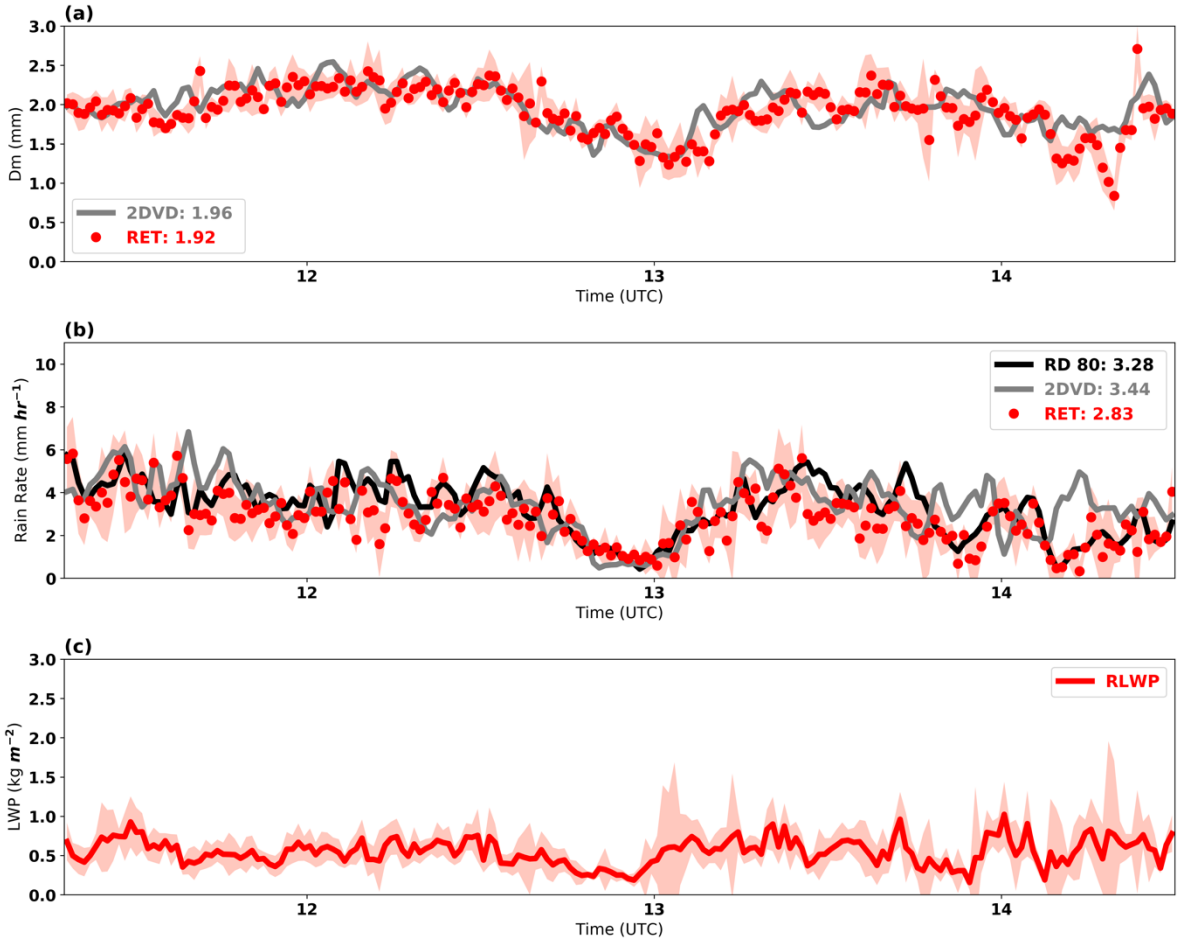

Figure 4. Time series of (a) retrieved (RET) (red dots) and 2DVD surface disdrometer estimated (grey line) D_m, (b) RET (red line), 2DVD (grey line) and RD-80 (black line) surface disdrometer rain rate estimates, and (c) retrieved rain liquid water path (RLWP, red dots) for Case A (May 20, 2011. The red shading areas are the estimated retrieval uncertainties.

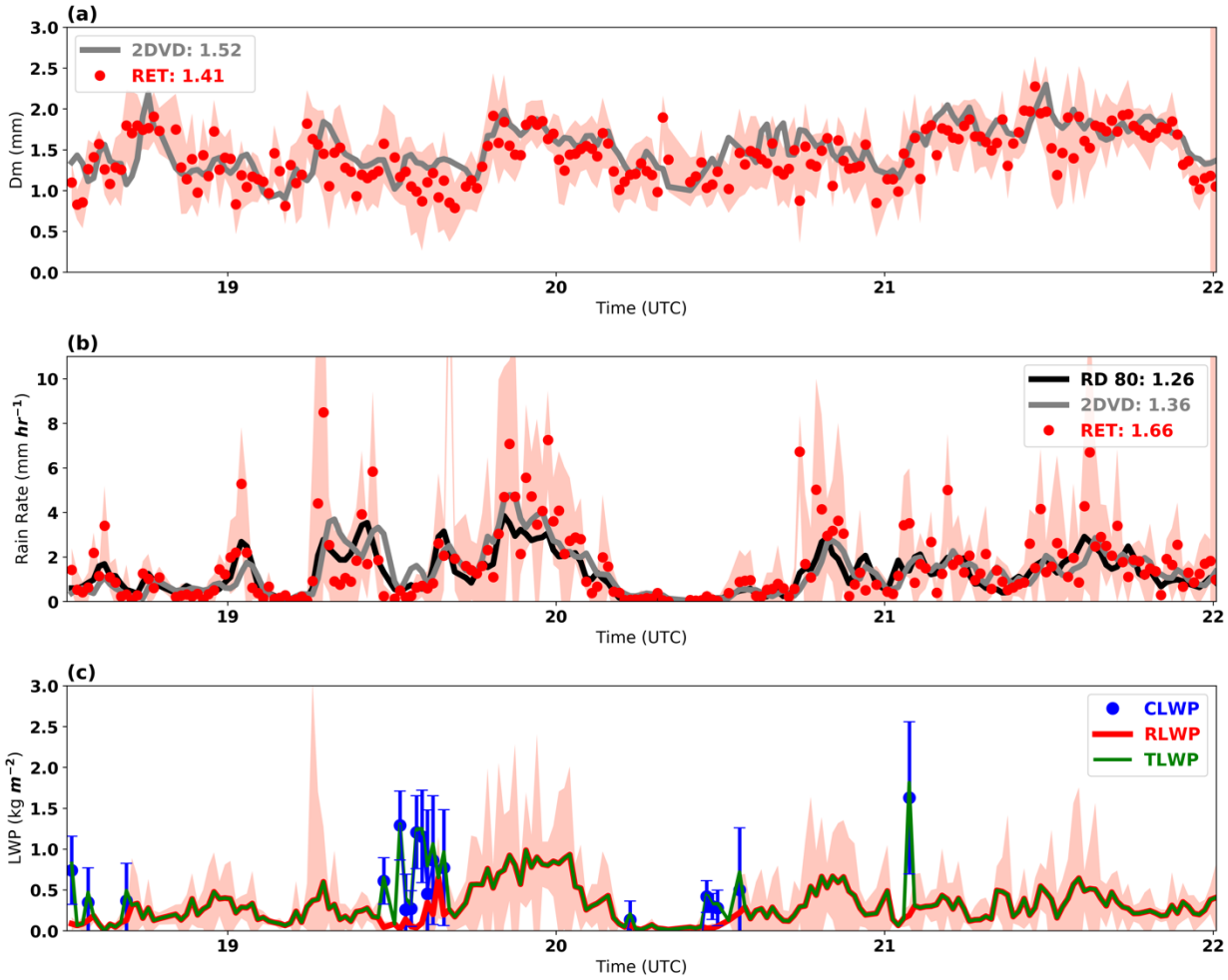

Figure 5. Time series of (a) retrieved (RET) (red dots) and 2DVD surface disdrometer estimated (grey lines) D_m, (b) RET (red dots), 2DVD (grey line) and RD-80 (black line) surface disdrometer rain rate estimates, and (c) rain liquid water path (RLWP, red line), cloud liquid water path (CLWP, blue dots) and liquid water path (LWP = RLWP+CLWP, green lines) for Case B (May 11, 2011). The red shading area and blue bars are the estimated retrieval uncertainties for rain microphysical properties (D_m, rain rate and RLWP) and CLWP.

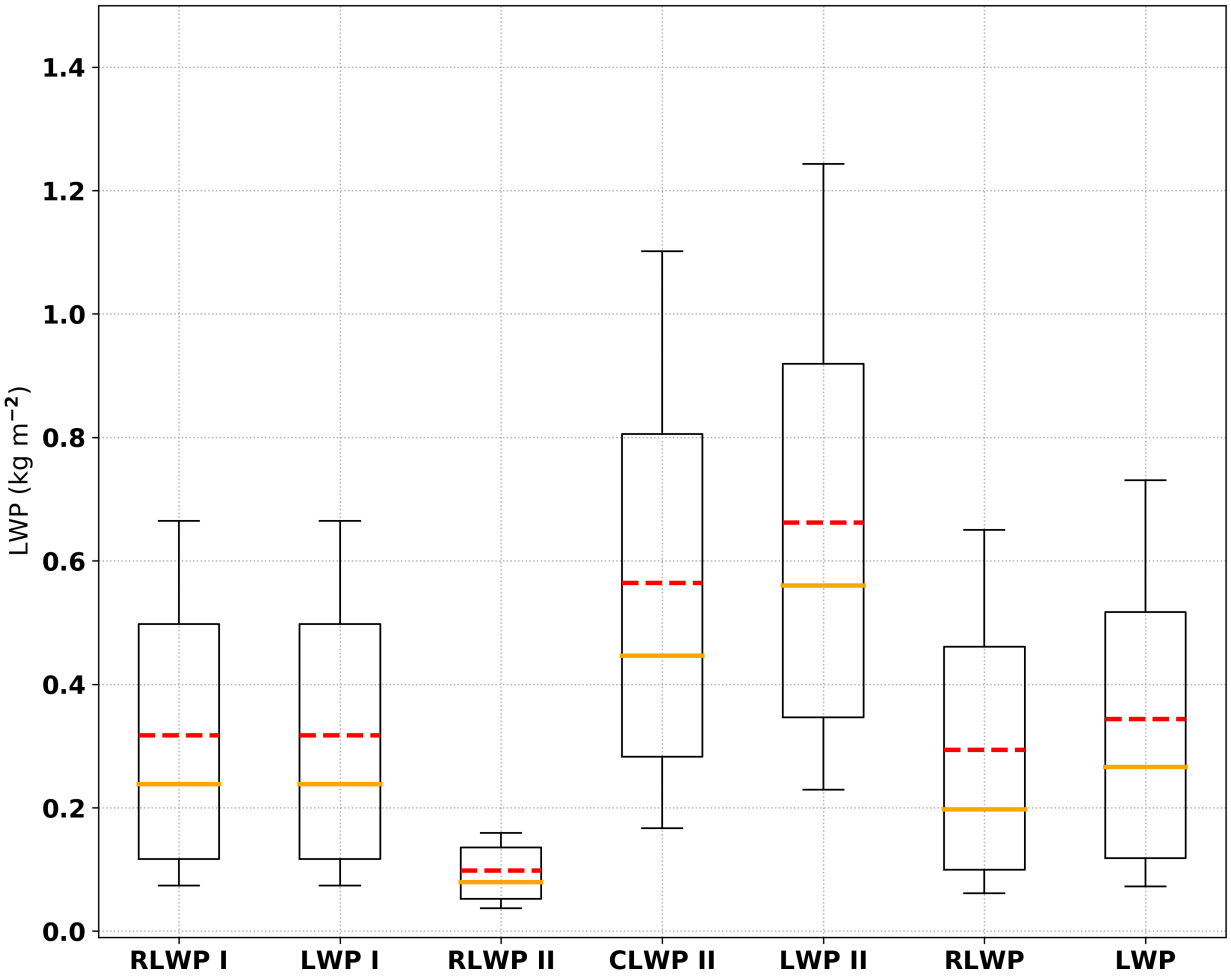

Figure 6. Box and whisker plots of retrieved RLWP, CLWP and LWP for situation (I), (II) and all samples. The horizontal orange line within the box indicates the median, boundaries of the box represent the 25th- and 75th -percentile, and the whiskers indicate the 10th- and 90th -percentile values of the results. The red dash lines represent the mean values.

729

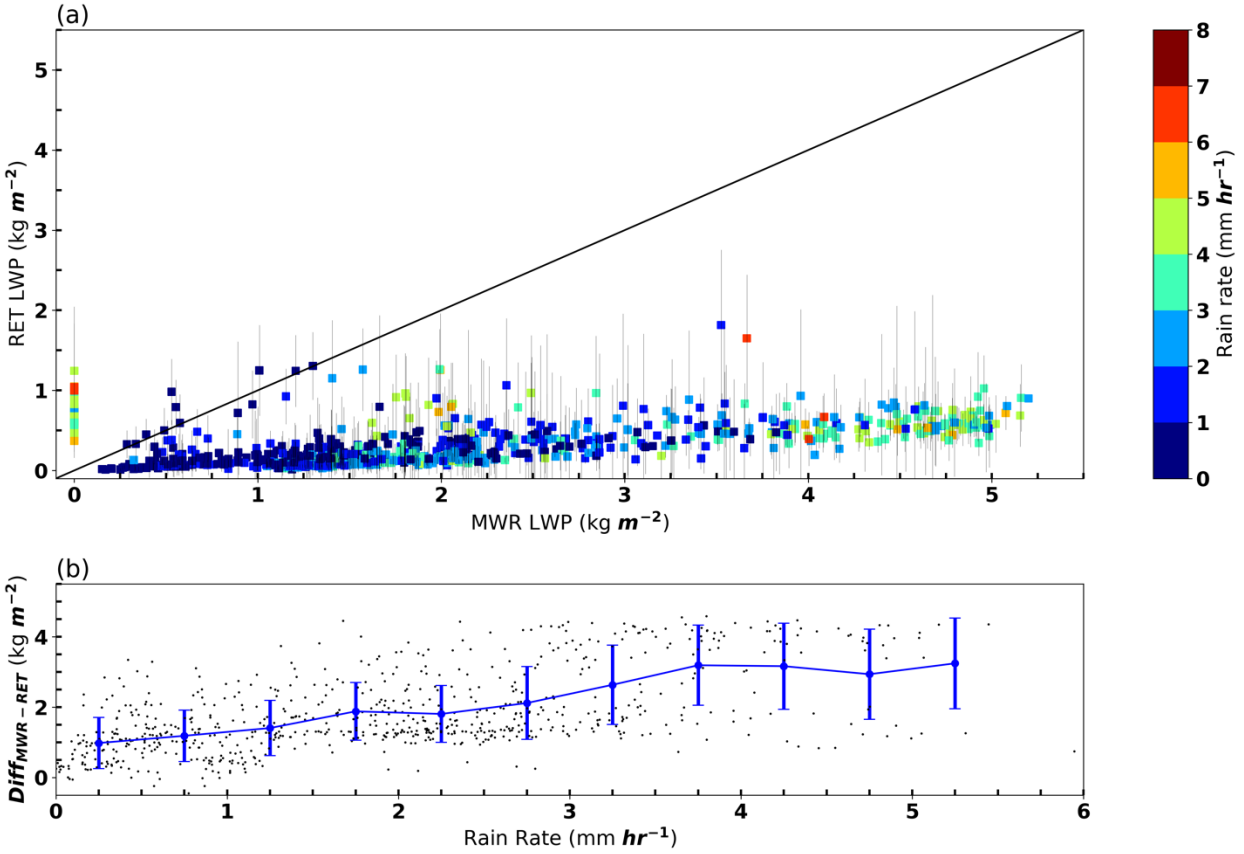

730

731 **Figure 7**. (a) Comparisons between LWP from microwave radiometer (MWR, in x-axis) and
732 LWP retrievals from this study (RET, in y-axis, with estimated uncertainty in gray lines). The
733 rain rates are indicated by colors. (b) the LWP differences between two estimations (MWR-
734 RET), shown as a function of rain rate.

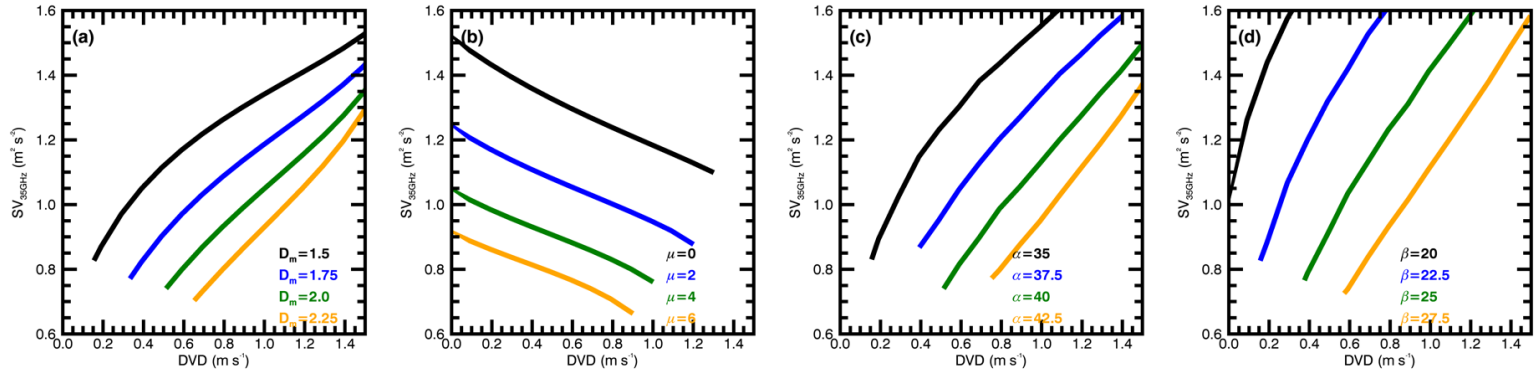

735

736 **Figure A.** Comparisons of (a) mass-weighted mean diameter D_m (mm), (b) shape parameter μ, (c) parameter α= 10 log(Z_{3GHz}/RLWC),
737 and (d) parameter β = 10 log(Z_{3GHz}/RR) calculated as functions of Doppler velocity difference (DVD) and spectrum variance at 35
738 GHz (SV_{35GHz}). Note that the units of RLWC and RR are g m^{-3} and mm hr^{-1}.

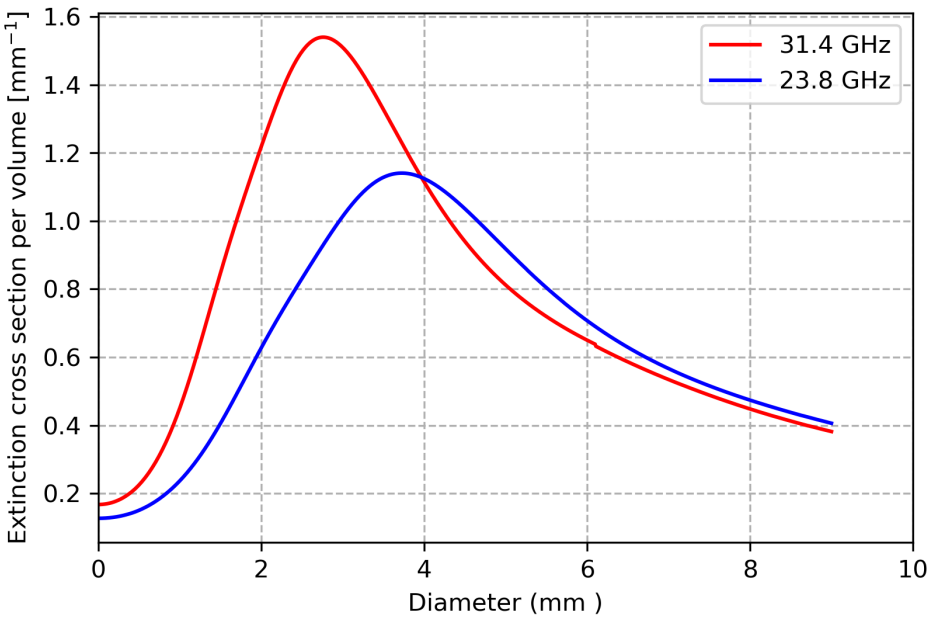

739

740 **Figure B.** The extinction cross section per volume as a function of the drop equivolume diameter for the two frequencies in MWR (23.8 GHz
741 and 31.4 GHZ).

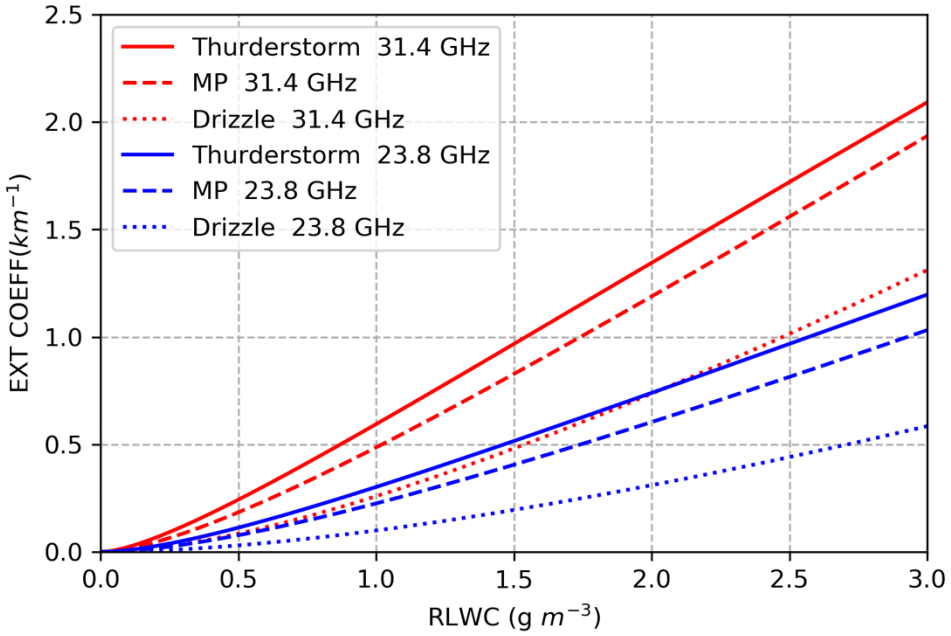

742

743 **Figure C.** The extinction coefficient as a function of RLWC for precipitations with three different drop size distributions (DSDs), which are for
744 heavy precipitation (thunderstorm), moderate precipitation (MP) and drizzle precipitation (drizzle).

745
746